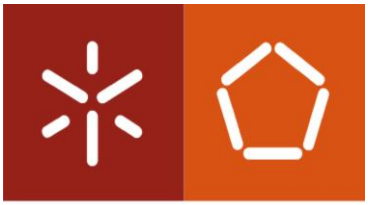

Universidade do Minho
Escola de Engenharia

Miguel Campos Nogueira

Wireless Power Transfer with a Wireless Communication Co-design

Dissertação de Mestrado
Mestrado Integrado em Engenharia Física
Área de Especialização em Dispositivos, Microssistemas e Nanotecnologias

Trabalho efetuado sob a orientação do
Professor Doutor Paulo Mateus Mendes

Julho de 2018

AGRADECIMENTOS

Na realização da presente dissertação, contei com o apoio de diversas pessoas e instituições às quais estou profundamente grato. Quero agradecer, em primeiro lugar, ao meu orientador, o Professor Doutor Paulo Mateus Mendes, pelo projeto proposto, pela orientação prestada, pela paciência, pelo tempo que investiu em mim, pelos ensinamentos, pela disponibilidade que sempre demonstrou, pela experiência e por me ter dado a oportunidade de integrar o projeto LiDAR na Instituição Bosch.

Aos meus pais José Alberto e Custódia Maria, o mais sincero obrigado pelo amor, carinho, motivação e dedicação ao longo da minha vida. O que sou hoje também é graças a vocês.

À minha família mais próxima, nomeadamente aos meus avós, aos meus padrinhos, aos meus tios e primos, fica um agradecimento pelos bons momentos ao longo de toda a minha vida e pelo apoio durante estes cinco anos.

Aos meus amigos e colegas do laboratório de Gualtar e da equipa LiDAR, agradeço o excelente ambiente de trabalho, os conselhos, as discussões e a entreajuda. Em particular, ao Pedro e ao Hugo agradeço o apoio e as discussões no âmbito desta dissertação.

Esta dissertação foi realizada na Bosch no âmbito de uma parceria de projetos de inovação, por isso agradeço à instituição e aos meus colegas de trabalho por me terem acolhido e ajudado ao longo deste percurso. Com um especial agradecimento ao Alexandre, pelo seu apoio e ajuda na elaboração do projeto.

Por último, mas não menos importante, quero agradecer à minha namorada por me apoiar sempre que preciso, por me dar força e encorajar quando estou cansado ou desmotivado, pelo amor, e pelo companheirismo que partilhou comigo nos últimos anos e pela ajuda prestada durante a realização da presente dissertação.

RESUMO

Hoje em dia, com o surgimento dos veículos autónomos, sistemas LiDAR (*Light Detection and Range*) começam a surgir e sensores LiDAR rotativos são usados para avaliar o ambiente que envolve o veículo. Graças ao seu movimento de rotação, a remoção de conexões físicas é de extrema importância. Portanto, métodos que transferem energia e dados sem fios para o sensor LiDAR são de grande importância.

Nesta dissertação, foi proposto um *co-design* entre um sistema de transferência de energia sem fios (WPT) e um sistema de comunicação sem fios, que vão fazer parte do sensor LiDAR rotativo. A transferência de energia e dados entre o automóvel e a parte rotativa é crucial, devido ao facto dos componentes existentes no lado rotativo precisarem de ser alimentados para recolherem informação sobre o que rodeia o veículo e enviá-la para o centro inteligente do automóvel. Considerando que o sistema vai estar no veículo, o *co-design* vai ter de cumprir especificações muito particulares, tais como as dimensões, o alcance sem fios (por volta de 10 mm), a potência entregue (entre 25 W e 50 W), a velocidade de comunicação (no mínimo de 6,5 Mbit/s), a gama de temperaturas (entre -40 ºC e +85 ºC), e a conformidade EMC.

Como o espaçamento sem fios é de 10 mm, foi adotado um método de campo próximo para a transferência de energia sem fios, o acoplamento indutivo. Para avaliar a performance das bobines de transmissão e receção utilizadas neste método, foi utilizado o software HFSS. Esta avaliação determina a influência do número de voltas, do raio interno e externo, do número de camadas e da separação entre voltas na indutância própria e indutância mútua das bobines. Outros testes foram feitos para avaliar a influência da distância entre as bobines, do desalinhamento lateral e angular, da presença de um veio no meio das duas bobines, da presença de obstáculos perto das bobines e de diferentes *designs* de ferrites na indutância mútua e indutância própria das bobines.

Foram especificados e testados dois sistemas de transferência de energia sem fios, um contra o outro, para avaliar a resposta dos mesmos à variação da distância entre as bobines, à variação do desalinhamento angular e lateral e à presença de obstáculos perto das bobines. Um deles destacou-se em todos os testes e foi escolhido para ser utilizado no *co-design setup*.

A comunicação sem fios também tem uma bobine como antena, de modo a manter a comunicação protegida de perturbações externas e assegurar a imunidade ao movimento rotacional a que a antena de transmissão vai ser submetida.

Ambas antenas dos sistemas sem fios trabalham com campos magnéticos, e a antena de comunicação é colocada dentro da antena do WPT. Como resultado da grande diferença entre as frequências de operação dos dois sistemas, ambos trabalham em simultâneo sem interferir um com a outra. O sistema WPT final alcançou 81% de eficiência, para distâncias até 15 mm entre bobines. O sistema de comunicação alcança uma velocidade de comunicação de 6,75 Mbit/s, o que é superior aos pedidos 6,5 Mbit/s. Esta comunicação inclui todo o percurso dos dados: a informação flui do sensor LiDAR para o modulo de transmissão através de Ethernet, depois para o módulo Rx através de Wi-Fi e logo de seguida para a central de inteligência do automóvel por Ethernet. Estes resultados foram obtidos utilizando o *devkit* Olimex GATEWAY, que inclui o modulo ESP32-WROOM-32U com um conector U.FL para se poder ligar uma bobine como antena externa.

ABSTRACT

Today, when autonomous vehicles are becoming a reality, LiDAR (Light Detection and Range) systems have started to appear and as a result, LiDAR's rotative sensors are being used to evaluate all the surrounding environment of the vehicle. Due to its rotative motion, the removal of physical connections is of extreme importance. Therefore, wireless methods that transfer power and data to the LiDAR's sensor are of major importance.

In this dissertation, a co-design of a wireless power transfer (WPT) system and a wireless communication link, which is part of the rotative LiDAR's sensor, is proposed. The transfer of energy and data between the automobile and the specific rotative part is crucial, due to the fact that components on the rotative side of this sensor need to be powered in order to collect the vehicle's surrounding environment information and relay this to the automobile's intelligence centre. Considering that the system will be in a vehicle, the co-design deals with very particular specifications such as size, a wireless gap around 10 mm OTA, delivered power range from 25 W to 50 W, a minimum communication baud rate of 6,5 Mbit/s, a temperature range of -40 ºC to +85 ºC, and EMC compliance.

As the requested wireless gap is 10 mm, the inductive coupling was the adopted near-field method for the wireless power transfer system. To assess the performance of the transmitter and the receiver coils utilized to communicate in this method, a design was created in HFSS. This evaluation assessed the influence of the number of turns, the inner and outer radius of the coil, the number of layers and the separation between turns in the coils' self-inductance and mutual inductance. Other tests were also performed to assess the influence of the distance between coils, the lateral and angular misalignments, the presence of a shaft in the middle of the coils, the presence of obstacles close to the coils and different ferrite designs in the mutual inductance and self-inductance of the coils.

Two different wireless power systems were specified and tested, one against each other, to evaluate the response to the variation of the distance between coils, the variation of lateral and angular misalignments and the presence of obstacles near the coils. One of these excelled in all tests, which was then selected for the co-design setup.

The wireless communication also has a coil antenna that maintains the communication protected from external disturbance and to assure the immunity regarding the rotational motion of the transmitter side.

Both wireless systems' antennas work with a magnetic field, with their communication antenna placed inside the WPT antenna. As a result of the big gap between operating frequencies, both work simultaneously without interfering one with each other. The final WPT proposed system achieved 81% of efficiency, for distances up to 15 mm. The wireless communication reaches a full communication baud rate of 6,75 Mbit/s, which is above the requested 6,5 Mbit/s. This communication includes the full communication link: the flow of information from the LiDAR's sensor to the Tx module by Ethernet interface, then to the Rx module by Wi-Fi and then again though on Ethernet interface to the vehicle's central intelligence. These results were obtained with the Olimex GATEWAY devkit board, which includes the module ESP32-WROOM-32U with an U.FL connector to link the communication coil.

TABLE OF CONTENTS

LIST OF FIGURES

LIST OF TABLES

LIST OF ABBREVIATIONS AND ACRONYMS

AC	Alternate Current
BOM	Bill of material
CPT	Capacitive Power Transfer
DC	Direct Current
EM	Electromagnetic
EMC	Electromagnetic compatibility
ICWPT	Inductive Coupling Wireless Power Transfer
IPT	Inductive Power Transfer
LiDAR	Light Detection and Range
OTA	Over-the-air
RF	Radio Frequency
TCP	Transmission Control Protocol
WPT	Wireless Power Transfer

CHAPTER 1 INTRODUCTION

Currently, the number of functionalities presented in the automotive industry is increasing and as a result, LiDAR (Light Detection and Range) systems are appearing. With the evolution of these systems, a 360 º angled recognition is required. Consequently, the removal of physical connectors is imperative since the goal is for the system to rotate freely. Wireless Power Transfer (WPT) is one of the options to deliver power to the system wirelessly. To complete the wireless interface, a co-design communication is also important to transmit the information of the involving environment gathered by the LiDAR's sensor to the vehicle in real time.

1.1 Wireless power transfer

Nikola Tesla was the first to develop a method to transfer energy wirelessly. In the beginning of the 20th century, he utilized Electromagnetic (EM) fields to transfer energy over long distances. However, the technique was not successful due to the creation of large EM fields, which may be harmful to human health. Even so, he left a first impression on Wireless Power transfer (WPT). There are many different techniques to transfer power from the source to the load without any physical connection to the power supply, shown in Figure 1, which creates new possibilities to charge portable devices [1]. To achieve this, the energy is converted by a transmitter to an oscillating magnetic or electric field that propagates over-the-air (OTA). The receiving part operates in the opposite way by converting this field into usable electrical power to supply a device (load) [2].

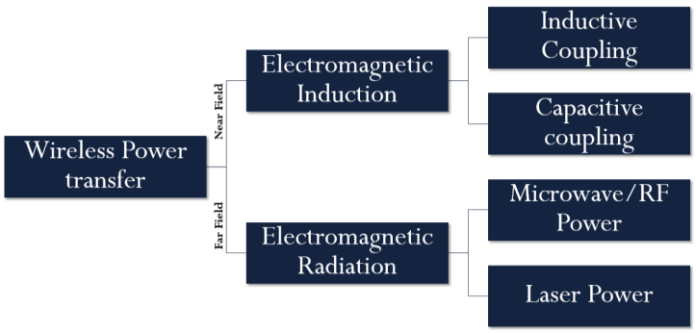

Figure 1 - Overview of WPT technology

Considering the distance between the antenna and a hypothetical receiver in Figure 2, the EM fields induced from the transmitter antenna assume different behaviours as they drift away, depending on their distance to the receiver. The operation region will depend on the size of the transmitter antenna as well as the wavelength of the emitted field, being possible to differentiate three regions. In the far field region, the ratio between the electric and magnetic field is designated as wave impedance. In fact, for mid/long range, the fields behave as quasi-static oscillating dipole fields [3]. To transfer energy over long distances (far field region), high-power lasers or microwave/radio frequencies (RF) are used [4]. As shown in Figure 2, there is a transition region between the aforementioned regions that continues to be part of the near field called Fresnel region or radiative near field which exhibits behaviours of both regions.

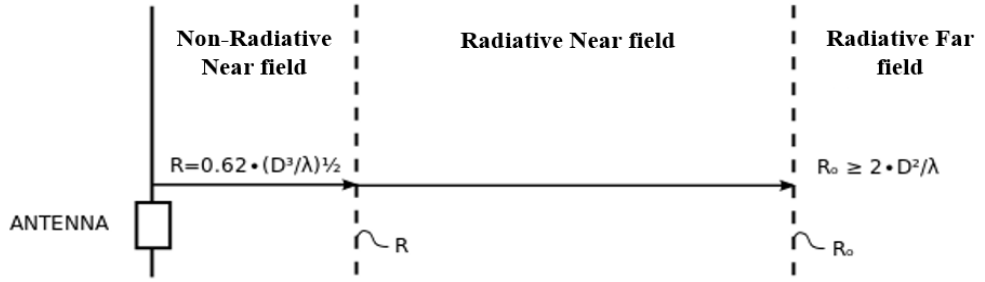

Figure 2 - Near field and far field regions for an antenna with diameter D that radiate a field with wavelength λ. Adapted from [5].

The main areas of application for this technology can be divided into [2]:

- Industrial (operation in rough environment)
- Automotive (battery charging and innovation systems)
- Aerospace (powering moving parts)
- Consumer electronics (charging mobile phones or laptops)
- Biomedical (power implantable biomedical devices)

The idea behind WPT in general is utilizing the capability of both electric and magnetic fields to transport energy. However, the receiver cannot utilize that energy if those fields are stationary. For WPT to work, it is necessary to utilize an AC source that will induce an oscillating field in the transmitter antenna. This field will induce an AC current in it (energy) which can be used to deliver power to a load [6].

Even though the same fields (electric and magnetic) are used in WPT as in wireless communication, different antennas may be usedwhere electrostatic and magnetic induction since the primary goal is the transferring of energy, instead of information codified in energy [4].

Technology	Range	Frequency	Antenna
Inductive coupling	Short	Hz-MHz	wire coils
Resonant inductive coupling	Mid	kHz-GHz	tuned wired coils
Capacitive coupling	Short	kHz-MHz	plate electrodes
Microwaves	Long	GHz	parabolic dished phased arrays
Light waves	Long	≥THz	lasers photocells

Table 1 - Properties of WPT technologies

Each type of technology will have a different range, frequency and antenna as shown in Table 1. Inductive and capacitive coupling are both in short range (near field) while microwaves and light waves are in the long range (far field). In the middle range, a specific type of inductive coupling where the coils are in resonance with each other is found. Considering the fact that the first two are the same forms of technology working in different conditions, it is possible to conclude that every different form of technology uses a different type of antenna that is adapted to the fields used in the transference of energy.

1.1.1 Non-radiative near field

This region is also called inductive near field because it is the region where electrostatic and magnetic induction dominates. In this region, the intensity of the electromagnetic field begins to wane with the cube of the distance between the WPT antennas, so that the distance will have a very importing role in the amount of transferred energy. This region is called non-radiative because the induced electric field does not radiate from the antenna without a presence of the receiver antenna in the capacitive coupling and because the magnetic field has closed field lines without the presence of the receiver in the inductive coupling. Therefore, the energy will not be lost or transferred without a receiver in both cases [7].

1.1.1.1 Capacitive coupling

In this type of coupling, the transmitter and the receiver antennas are represented by two metallic plates and likewise in a capacitor, transfer the energy by electric fields. In Figure 3 the electrode and the intervening space represent the metal plates and the dielectric in ordinary capacitors, respectively [8].

The transmitter plate converts, by electrostatic induction, an alternate voltage into an oscillating electric field (EF). When this field reaches the receiver plate, the opposite behaviour happens and an AC voltage is induced bringing back the alternate voltage [8]. The system capacitance is limited by the available area for the WPT system since the capacitance is proportional to the area of the smaller electrode and inversely proportional to the separation between them [9]. High voltage on the electrodes are required which can be dangerous, so this technique is commonly used only for low power applications [10].

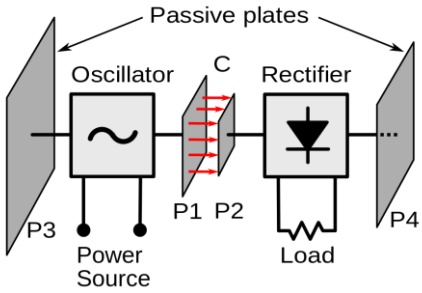

Figure 3 - Unipolar capacitive coupling [11].

As is well-known, the electric field interacts with materials in which the dielectric constant is different from the value 1. Therefore, when these materials were near the electrodes, they interacted with the electric field, which in this place disturbed the power transfer. The principal goal of this technique is to minimize this effect which in turn opens new doors to transfer energy between substrate layers in integrated circuits [12].

1.1.1.2 Inductive coupling

In the near field methods, inductive coupling is also a very good alternative and the most used technique. It consists of two separate coils in which the power can be transmitted through a magnetic field [13]. An alternate current (AC) source supplies current to a coil that will induce an oscillating magnetic field, as Ampere's law dictates. When this field reaches the second coil, the opposite behaviour happens and an alternate current is induced which delivers power to the load as shown in Figure 4. If the magnetic field does not find any secondary winding, the energy remains in the circuit because the magnetic field lines are closed. The main characteristics of delivering power with this technique is the short range (non-radiative near field region), since the electric and magnetic field's intensity decays with the fourth and sixth power of the distance respectively [6]. This method of operation is an example of a transformer functionality with the principal difference being that the coupling medium is a ferromagnetic material that is inside of both coils [14]. Nowadays, big companies use this method, as the oldest and most widely used WPT technology, as a conventional technique for WPT systems available on the market.

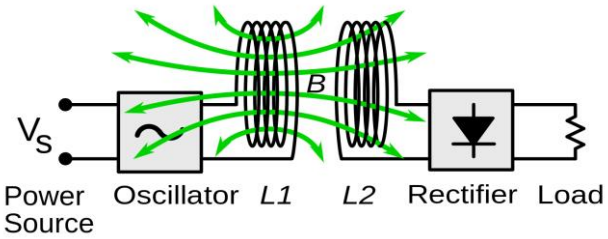

Figure 4 – Inductive coupling [11].

The method described above is not very efficient when transmitting energy for long distances because large amounts of energy are wasted by inductance of the WPT coil. By exploring some near-field interaction between the source and the receiver, there is a way to tune this system for an efficient power transfer. In coupled resonant systems, there are specific operation regimes where the transferred energy was expected to be the most efficient possible. By using coupled resonant circuits (same frequency), it is possible to reach longer distances of energy transfer due to the fact that they have a resonant connection [1]. Since the transmitter and receiving part work in resonance with each other, this results in a very efficient WPT system in which the resonant circuit is a coil connected to a capacitor which, when in resonant, cancels the impedance that makes the previous method less efficient. Figure 5 represents an inductive coupling system with two resonant circuits where the magnetic fields oscillate at the same frequency exchanging energy effectively [11].

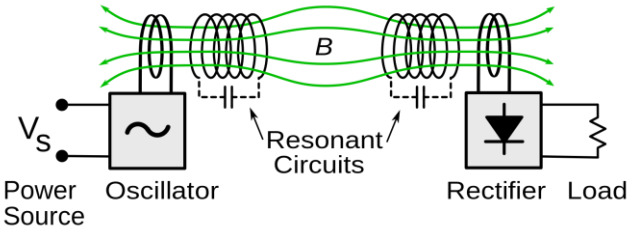

Figure 5 – Resonant inductive coupling with two resonant circuits to increase the distance [11].

1.1.2 Radiative far field

For large range energy transfer, other techniques arise. For long distances, it is necessary to use electromagnetic radiation like microwaves and lasers. In contrast to what happens in non-radiative techniques, radiative techniques send radiation in the presence or not of a receiver. The efficiency is limited by the cross section of the receiver antenna since the radiation spreads out from the transmitter antenna. Most of the radiation is sent towards other directions (lost energy), mostly in omnidirectional systems. Even in unidirectional radiation sources like Lasers, these might have some issues since an uninterrupted line of sight and an alignment mechanism is needed [15].

1.1.2.1 Microwave

In this method, the energy is transmitted by a well-focused microwave beam. To proceed into this type of WPT (shown in Figure 6), a transmitting antenna is needed to emit microwave radiation and a combination of receiving and converting unit called "rectenna" to reconvert the beam to DC. This last part could reach highly efficient conversions. However, this technique increases the health risks caused by the focused radiation [14].

In [16], Geoffrey talks about a solar power system using a microwave beam at 2.45 GHz in which the satellites have a transmission antenna with 1 kilometre of diameter and a receiving rectenna with 10 kilometres of diameter. For lower frequency systems, the size of the antennas needs to be increased.

Figure 6 - Project of the solar power system based on a Microwave WPT [14].

Due to the high dispersion of the microwave beam, to catch all the radiation, the rectenna must be bigger than the transmitter antenna. For longer distances, the size of the rectenna needs to be increased too, or some radiation will be lost, which in turn, will decrease the WPT efficiency.

1.1.2.2 Lasers

Far field WPT can also be achieved by using a laser emission beam. This technique is generally called “power beaming” because the energy is transmitted in the form of a beam until it reaches a receiver which can convert it back to electrical energy. Like laser suggests, the beam is collimated and monochromatic which allows a narrow beam cross section with high intensity and, consequently, a compact receiver antenna. However, Laser radiation is very dangerous for humans and other animals, so it needs a direct line of sight with the receiver and the system efficiency which is limited by the existing solar cells [14].

Comparing the two far field techniques, microwave transmission is the most efficient since its technology allows for more efficient antennas, while the laser method is limited by the actual efficiency of solar cells.

1.1.3 WPT biological impact

Recognizing the WPT as a new technology with unknown health consequences, its viability and security needs to be ensured for all users. The human body is composed of biological tissues which have conductive properties, representing little antennas in the presence of strong EM fields. When these tissues are in such an environment, they oscillate in resonance with the emitted fields [14]. Due to the fact that WPT is a new and recent form of technology, there are no studies regarding the long-term effects of the impact of the specific absorption rate (SAR) in the user’s health when in close contact to a wireless power system (strong magnetic fields). Therefore, regarding the use of the WPT system in a LiDAR sensor, the WPT fields will remain only in the local, with an isolated environment to protect all the passengers in the automobile from radiations.

1.2 Wireless communication

Normally, this type of communication uses radio waves which have a very long range that depending on the protocol, could reach several thousand or even millions of kilometres. Light, magnetic, or electric fields could also be used to communicate wirelessly but are not so common. The transmitter converts the message into a RF Signal (for example a radio wave). In

the receiver side, the RF signal is converted back to the message as Figure 7 shows. To assure the correct message reaches the receiver, some communication rules, called protocols, are set. These protocols allow entities to transmit information between them (two or more) with the same "language". They also guarantee the synchronization of the communication and the possibility of error recovery methods. Wireless communication error recovery methods are of extreme importance since the exchanged information is more susceptible to getting lost because it travels without an electrical conductor [17].

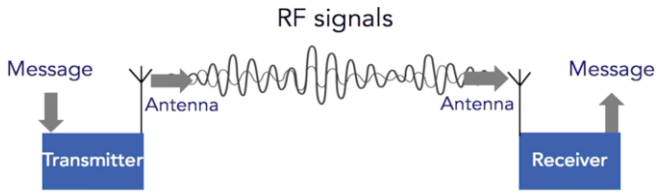

Figure 7 - Schematic of a wireless communication [18].

To communicate, a transmitter relays the data to the receiver, as represented in Figure 7 however, most of the times, a single entity is two together, and the information flows in both directions as suggests the Figure 8.

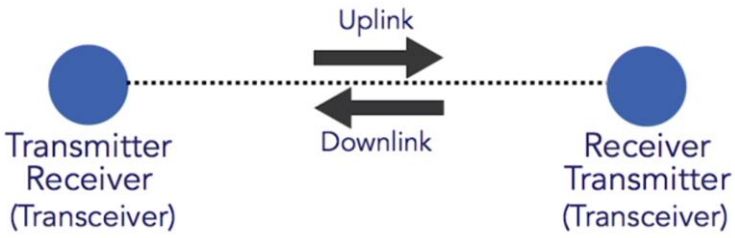

Figure 8 - Representation of a communication in both directions [18].

In contrary to what happens with WPT, this technology experienced a strong development process during the 20th century. To communicate wirelessly, it utilized different types of signals as Radio frequency, Infrared, Microwave and Lightwave.

In Figure 9, the main Wireless communication protocols present in the Radio Spectrum are represented. Considering information will be carried from the device to a receiver in the vehicle, it must occur only at short distances with a maximum of 8 centimetres. The LiDAR system will require a high sending speed taking into account the number of points per second that are intended to be sent, with 10 MHz being the lowest frequency allowed. The safety of communication should also be ensured since the information will contain the "vision" of the automobile. Regarding the previous considerations, it is of interest to provide an overview of some of the communication protocols.

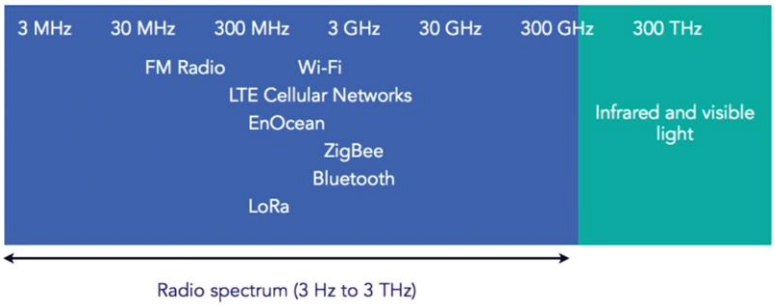

Figure 9 - Radio Spectrum [18].

1.3 Motivation and aim of the dissertation

Nowadays, the term of autonomous vehicles strongly appears in the automotive industry, making many companies compete to obtain the best performance with high level of driving safety. Even with the existence of some vehicles with that feature on the market, the challenge remains, since they are not completely autonomous. The main characteristic that needs some work is the “vision” of the vehicle because this technology suffers some issues in recognizing the automobile’s environment. The vehicle’s 3D image creation system involves the union of three technologies, namely the radar and the infrared camera, that are already being used in autonomous vehicles, and LiDAR. The aim of this dissertation is to deliver power and to communicate with a LiDAR sensor.

The LiDAR measures the distance to objects by illuminating the target with a pulsed laser light and measuring its reflection with a sensor, resulting in a precise 3D image of the

environment around the automobile [19]. The high speed at which the image is acquired allows the sensor to obtain a 3D image of the whole surrounding environment, even when the vehicle is travelling at high speeds.

In a sensor capable of having a 360 º viewing angle working in constant rotation, it becomes impossible to have cables powering the system and communicating with it. The aim of this work is to build a small WPT capable of transferring enough energy to feed the LiDAR's sensor and a wireless communication co-design that needs to support high transmission data rate to send the information obtained by the LiDAR's sensor to the central intelligence of the vehicle.

This dissertation has been developed alongside the LiDAR's system project, whose specifications are constantly adapting according to tests and new variables. The initially required specifications were a maximum board and coil size of (60*60*20) mm^3, a temperature range from -40 ºC to 85 ºC (automotive requirement), the capacity to deliver between 25 and 50 W and with a baud rate of 6.5 Mbit/s. These requirements could change during the dissertation to adapt the LiDAR's system. However, during the development work, the requested power was at least 40 W and the maximum allowed length decreasing from 60 mm to 40 mm. The actual method to make the LiDAR's sensor rotate was not defined until the end of the dissertation. However, two strong possibilities remain in which one of them is to use a shaft that passes through both coils that will enhance the coupling between them.

1.4 Contributions

In this dissertation, a wireless power transfer with a wireless communication co-design was proposed. This design was optimized to reach the highest efficiency possible taking into account the available size and possible LiDAR designs that can interfere with the power and data transfer. After defining a module of the coils in HFSS, different WPT systems were tested, confirming the results.

The tests were made towards finding an optimal coil format for the LiDAR application (Figure 10). These tests were shared with the whole LiDAR team to design the final system with the best WPT neighbour systems and an appropriate shaft material and size.

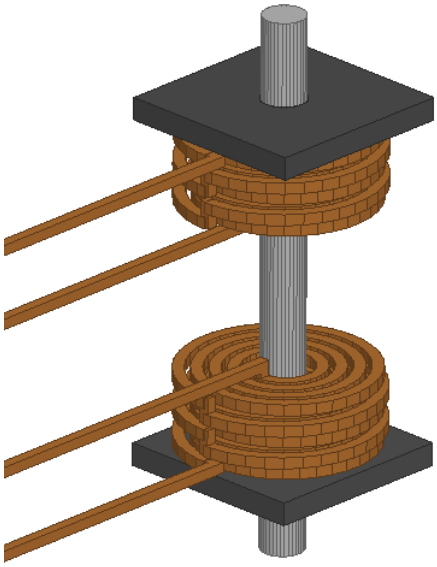

Figure 10 - Final simulation's design of the WPT coil with a shaft.

The wireless communication antenna will utilize a magnetic field to communicate instead of an electromagnetic field as the conventional ones. The antenna will have a design of a flat coil as the wireless power transfer antennas, as shown in Figure 11.

Figure 11 - Communication antennas

A co-design between both wireless systems was proposed with the wireless communication antenna inside the inner radius of the WPT antenna. In Figure 12, the final co-design setup is represented

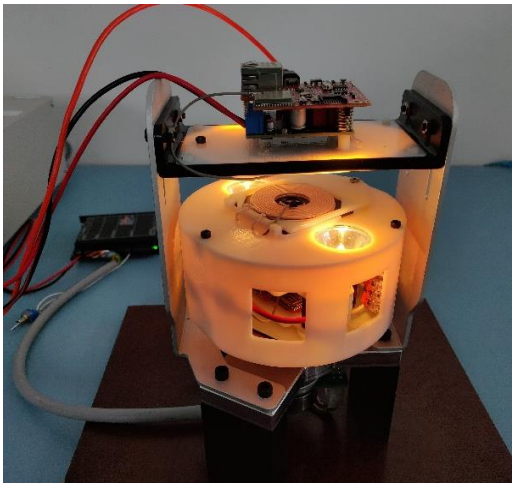

Figure 12 - Final setup.

1.5 Outline and structure

This dissertation is composed of 5 chapters, each one representing a part of the developed work.

Chapter 1 is an introduction to the problem to be tackled in this dissertation. It also introduces the concepts of power and data transfer wirelessly, and the aims and contributions of this dissertation.

Chapter 2 contains the state of the art of small and high power WPT systems, alongside small and high data rate wireless communication. It also presents the state of existing co-design systems.

Chapter 3 contains the coils' simulation in HFSS in order to study the influence of the coils' parameters and optimizes them to have the best performance in this specific application.

Chapter 4 presents the real wireless power system capable of transferring 50 W with high efficiency and a co design with a wireless communication system.

Chapter 5 contains the conclusion and future work of the dissertation.

In the appendixes, the wireless communication code of the Tx and Rx module are presented.

CHAPTER 2 WIRELESS POWER TRANSFER AND WIRELESS COMMUNICATION

In this Chapter, wireless power and data transfer systems will be reviewed to better understand the main problems of the existing systems and to compare them according to their applications. Regarding the aim of the dissertation, the co-design between these two wireless systems will be considered. Methods to optimize the efficiency of the system will also be reviewed.

2.1 High tower transfer

The review will be focusing on the aforementioned WPT near field techniques, which have been experiencing a high-speed development period in the recent years. Regarding the system requirements, only the solutions that can transfer at least 10 W will have importance, even if low power systems (less than 25 W) cannot be used. Different techniques could have been applied in these low power systems that could help them avoid temperature or size issues.

2.1.1 Capacitive coupling

Capacitive Power Transfer (CPT) had been forgotten until 2008, but then it regained the research community's attention, as it was a non-radiative form of power transfer as mentioned in the previous chapter. Following the literature, this technology is in use for biomedical technology instruments [20], for portable and wireless chargers applied to consumer electronics [21] for automotive applications [22] among others. Until this time, mostly low power solutions were found for this type of coupling regarding the required small size. In [23], a 30 W capacitive wireless power system was prototyped and studied with metal plates of 5*5 cm^2 over an air gap of 5 mm. It also reports a 20 times greater power deliver when compared with similar coupling capacitance in the literature, proposing a new capacitive WPT architecture as shown in Figure 13. Although in [22], a 350 W system with 70% of efficiency was achieved at 11 cm with very large plates with dimensions of 45*45 cm. The proposed system is intended to charge an EV, limiting the RMS voltage on the vehicle chassis to 132 V with intended further work to reduce it.

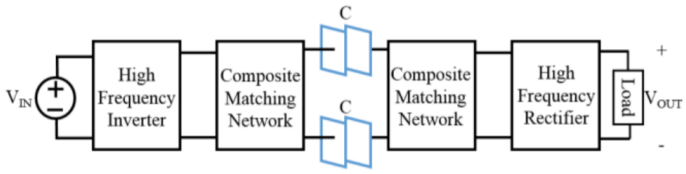

Figure 13 - Architecture of a capacitive WPT [23].

Commercially, the company Murata, produces a product that includes two modules (receiver and transmitter) for capacitive coupling WPT as shown in Figure 14. It uses two thin asymmetric electrodes dipole that can transmit 10 W of power OTA. The equipment may be powered by having a transmission (Tx) module in the recharging side and a reception (Rx) module in the equipment that will be powered. Their configuration has a high efficiency and position freedom [24]. The size of the modules, the efficiency and the distance at which the 10 W is transferred are unknown.

Figure 14 - Murata WPT equipment [21].

Each part of the module (transmitter and receiver) has one plate and when both are close enough to generate a capacitance, it allows the energy to be transmitted by an induced electric field. The reception module, consisting of a rectifier and voltage converter powers a device with direct current. The material between the plates (normally air) works like the dielectric in a capacitor [21].

The previously referred to CPT's systems make this technology very attractive for usage and with a huge potential. It has minimum EMC issues, can transfer power over metal barriers, under certain conditions, and can have power and data transferred simultaneously at the same frequency [25]. Although, it is a recent form of technology, when compared to IPT, which has better efficiency and easier coupling conditions, the CPT is usually used in low power applications [25].

2.1.2 Inductive coupling

IPT is the most common and utilized method to transfer power wirelessly in near-field region. After many efforts devoted by Tesla early in the 20th century, this technology was forgotten for several years, yet in the last years, it has risen again. In the 1970s, inductive power transfer was reinstated through academic studies [26].

In [7], a mechanism based on strongly coupled resonances for the modern world applications is proposed, including macroscopic and microscopic ones. The related applications could be used to power robots and mobile electronics and also autonomous Nano-objects by implementing this technique to CMOS technology and others.

An overall system with an efficiency of 82% capable of delivering 36 W with 5 mm between coils was developed in [27]. The coils size was unknown but following Figure 15, it is concluded that the size was above the required coil size presented in chapter 1.

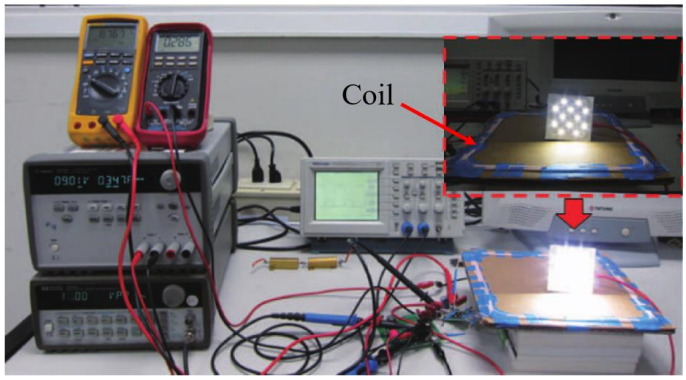

Figure 15 - Measuring setup of the system in [27].

This system was able to reach a good level of efficiency by adopting a Class-E amplifier instead of a Class-D. The coils are designed to obtain the best system performance and are made of litz wire. They also reduce the power loss utilizing high quality passive components. In [28], an 120 W WPT for a wireless automobile seat was proposed. With these applications, it is possible to power the car's seat wirelessly to heat, move and to make tilt adjustments as Figure 16 demonstrates. This system obtains a 55% efficiency over 20 mm of distance between coils. The coil's size and design were made to compensate the movement of the seat maintaining the efficiency by utilizing a two-layer spiral resonator of 150*120 mm^2 each.

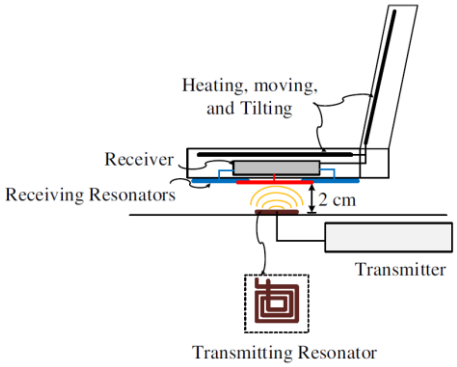

Figure 16 - Schematic of the Automobile seat in [28].

In [13], a system capable of delivering 60 W over 2 meters with coils which radius is about 8 times smaller than this distance using strongly coupled magnetic resonances with approximately 40% of efficiency is proposed. In [29], a small and helical coils approach was studied to power an EV which adapts the resonant frequency between two values depending on the distance, in order to maintain high efficiency for small changes in the relative position between the Tx and Rx. This system is capable of delivering 100 W with an efficiency of 97%, with a distance between coils of 100 mm. The system's antennas are two coils with 300 mm of diameter.

As the most utilized WPT, there are many available commercial options. In the following pages, the ones that met the best requirements will be shown.

Power Republic is only dedicated to the wireless power transfer systems and has 3 family products (PRX-2000, PRX-5000 and PRX-9000). Each family achieves a different type of power that goes from 5 W to 2 kW. The one that better fits the initial requirements of the proposed system is the PRX-2000. This product can transfer a maximum energy of 60 W with various coil sizes depending on costumer's products and with a high efficient WPT for low distance. The maximum distance supported by the system to continue to transfer energy is 30 cm with a maximum output of 5 W. The company also supports evaluation boards for initial testing by the customer in which efficiency, size and temperature range will depend on each case. Considering Figure 17, that represents the schematic of the PRX-2000 system, there are two types of transmitters with different inputs. The PRA-2000 receives an alternate current and the PRD-2000 receives a direct current [30].

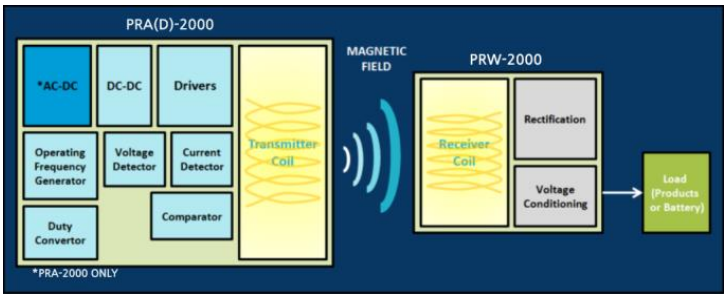

Figure 17 - Schematic of the PRX-2000 Family of Power Republic [30].

Power by Proxi was created to provide wireless power solutions to the market. They have designed a product (PM100) capable of transferring a maximum of 100 W. The size of this product has been optimised and is available in an 80*80*40 mm^3 package, with a 65 mm diameter and 20 mm width power coil (Figure 18). The system delivers a maximum of 91% efficiency for power transfers with distance between coils of 4 mm, ensuring no overheating. Recently they have also created a version with 150 W, but it is much bigger than the PM100 that is already above the limit purposed in the initial requirements. As the power of the first product is sufficient, this bigger option is not appropriate [31].

The system does not work for distances between the Transmitter and the Receiver longer than 41 mm. The product operates between -40 ºC and 70 ºC and uses a transmission frequency of 200 kHz. Currently (after the state of the art research), the company's products are no longer available, as their company was acquired by Apple and their technology adapted to Apple products [32].

Figure 18 - PM100 product of Power by Proxi [31].

IDT's wireless power products have lower output power values when compared with the required ones, that go from 5 W to 15 W. The P9242-R (transmitter) and P9221-R (receiver) can transfer 15 W between them using induced magnetic fields. By using a programmable current limit, an over-voltage developed by them and decreasing the number of required capacitors, they can reduce the cost of the device. The system operates between 0 ºC and 85 ºC and is immune to water, dust and other contaminations. The system's maximum efficiency is 81%, which is very good regarding the lower size advantage. The receiver's size is 26,4*39,4*6 mm^3 and the transmitter's size is 60*60*9 mm^3, both including the board and the coil. The most important advantage of the system is the communication module present in their devices, which allows the transfer of data and power simultaneously.

Ferro Solutions develops an inductive power system, presented in Figure 19, with a 390*276*89 mm^3 transmitter capable of transferring 60 W of power. However, it only offers small receiver options with dimensions of 12*12*3 mm^3, capable of receiving a maximum of 500 mW per unit with a distance of 28 mm to the receiver and ensuring continuous power (200 mW) over a maximum distance of 75 mm with unknown efficiency. The transmitter uses a pending antenna to obtain a homogeneous magnetic field on the top of the transmitter board and sends power to several devices simultaneously. This system also supports wireless communication (Bluetooth). The transmission frequency band is 127-130 kHz and the transmitter temperature range is from 0 ºC to 35 ºC [33].

A B

Figure 19 - Transmitter (A) and Receiver (B) [33].

Würth Elektronik developed some low and high power WPT technologies. Their most sold WPT could deliver 15 W of power [34]. However, they have also done some research in the area developing some different circuits for high power WPT systems using circuit technology. In their research note 032 [35], they present many different and small circuits that can accomplish the WPT process with high accuracy and efficiency. Their power delivering options go from 30 W to 100 W. They also make the board files available for two of those circuits (50 W and 100 W). In Figure 20, the 100 W system is presented. Considering the requested power presented in the previous chapter, the 50 W option will be available, with sizes of 54,4*46 mm^2 for the board and 53*53 mm^2 for the coils. However, there is a lack of functionality information for the maximum efficiency for a given distance. Considering the power and size of this system, it will be tested by printing the PCB and purchasing the components to produce the final board. The temperature of the system ranges from -20 ºC to +65 ºC however, due to the available board files, some components could be altered to accommodate temperature requirements.

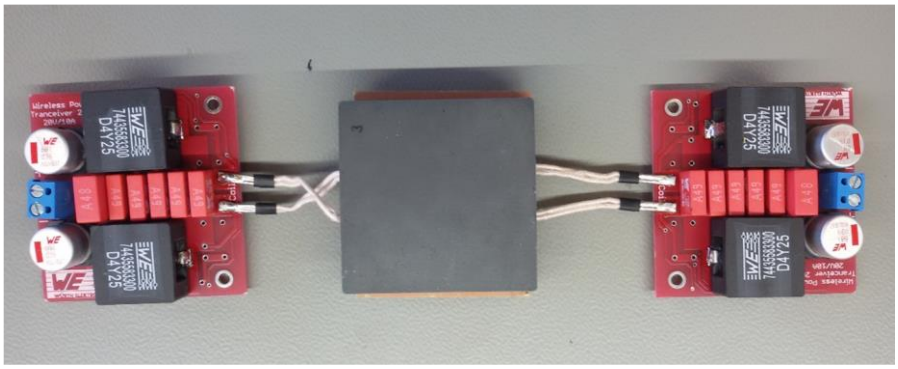

Figure 20 - Würth 100 W System [35].

Table 2 - Comparison between the commercial options

Company	Temperature Range	Output Power	Size
Murata	Unknown	10 W	Unknown
TDK	-30 ºC to +70 ºC	5 W	Coil: 32*48*18 mm^3 Module: 32*76*18 mm^3
Power republic	-20 ºC to + 60ºC	60 W	Depends on the device
Power by Proxi	-40 ºC to +70 ºC	100 W	80*80*40 mm^3 package with a 65 mm diameter coil
IDT	0 ºC to +85 ºC	15 W	Receiver: 26,4*39,4*6 mm^3 Transmitter: 60*60*9 mm^3
Ferro Solution	0 ºC to +35 ºC	60 W Tx 0,5 W/Rx	Receiver: 12*12*3 mm^3 Transmitter: 390*276*89 mm^3
Würth Elektronik	-20 ºC to +65 ºC	100 W	Coils: 53 mm of diameter Tx/Rx: 54,4*46 mm^2
Requesitos	-40 ºC to +85ºC	50 W	Coils: 60*60*20 mm^3 Tx/Rx: 60*60*20 mm^3

In Table 2, several high power wireless systems were reviewed but almost all of them have dimensions larger than required. Each one of the systems presented in the table has its advantages, however, none of them features all the requested specifications presented in the previous chapter. Considering the miniaturization and the required high power, some of them could be excluded. Regarding the Würth Elektronik, it is by far the better option since they send the PCB designs, leaving some freedom to adapt the system to fit all the requirements. On top of this, they also have a small PCB design with high power transfer.

2.2 Efficiency optimization

There are many parameters to take into account while improving the efficiency of a WPT maintaining a high-power transfer with a small system. The most significant improvements will be presented below.

The coil material is an important factor that could influence heat loss and the coil quality factor which is normally copper. However, for high power and frequency, the resistance of the material will be high enough to reduce the efficiency. To increase the efficiency, a litz wire is used, which has less resistance than solid copper, since it is composed of multiples insulated strands of copper as Figure 21 suggests.

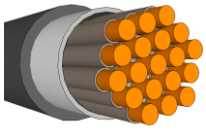

Figure 21 - Litz wire cable

Some materials between the coils could enhance the magnetic flux and consequently the efficiency of the system. Metamaterial is composed of artificial structures in order to acquire peculiar electromagnetic properties that could be advantageous for some applications. This type of material presents an isotropic negative permeability [36]. Normally, the metamaterial size needs to be in the same order of magnitude of the wavelength of the radiation used to transfer power, represented in Table 3:

Table 3 - Electromagnetic field wavelength as a function of the frequency.

Operating Frequency	Wavelength
10 kHz	30 Km
100 kHz	3 Km
1 MHz	300 m
10 MHz	30 m
50 MHz	6 m
250 MHz	1,2 m

Generally, WPT operates at frequencies in the order of 100 kHz-10 MHz, therefore a large metamaterial (3 km – 30 m) is necessary. The major challenge of designing this type of material at relatively low frequencies (MHz regime and lower) is their size. However, there is a way to use small metamaterial for these operating frequencies. If the metamaterial inductance was significantly increased, it would be possible to obtain some magnitude orders smaller than the wavelengths (called sub-wavelengths metamaterial) [37].

This type of technique is utilized for several centimetres of distance between the coils because the metamaterial helps focusing the magnetic flux into the secondary coil. However, in order to apply this type of solution, it is necessary to implement an object (metamaterial) between the coils obtaining the best results in the middle of the path [37].

Normally this material has some centimetres of depth and is utilized for mid and far field efficiency optimization. Research demonstrates that thinner metamaterials exist and that they have better results than an air gap for distances over 4 centimetres as demonstrated in Figure 22 [36]:

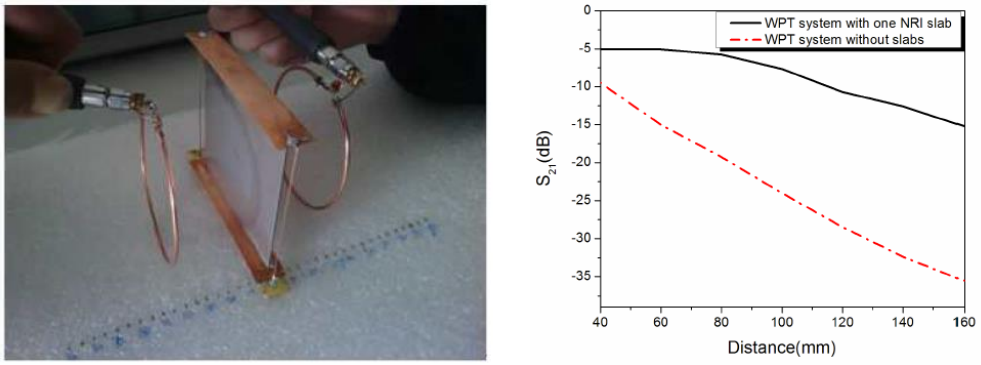

Figure 22 - In the left image, a WPT system with a metamaterial is presented; in the right image the dependance of S_{21} with the distance of that same system with and without a metamaterial is represented [36].

In [38], they propose another material that will be between the coils. The idea behind this technique is the same as with magnetic resonant inductive coupling where the coils are tuned. By utilizing a magnetic resonance field enhancer (MRFE), it is possible to increase the magnetic flux that reaches the receiver coil. This MRFE is formed by a wire loop connected with a capacitor, which has the same resonant frequency as the WPT system. This results in the increase of the transmission efficiency even higher than using metamaterials as shown by

Figure 23. The radius of the coil was chosen to maximize the enhancement (using a simulation). For this solution, the same problem of the previous technique is met. The implementation of an object in the middle of the path, so it is only utilized for middle/far-field implementations, is required.

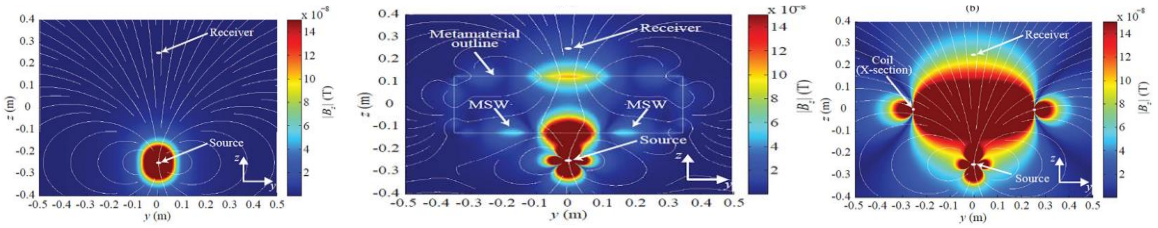

Figure 23 - Cross sectional magnetic fields of a WPT system with air only (left), a metamaterial (middle) and a MRFE (right) between the coils [38].

The coil can have many geometries, such as circular, rectangular, hexagonal, etc. The coil with the best ratio between inductance and occupied area is the hexagonal coil, although diverse formats for particular situations could result in very different geometries. In [39], a new coil format (Figure 24) optimized for power transfer over multiple coils proposed. In [37], antennas with very high inductance by using multi-turn planar coils have been designed.

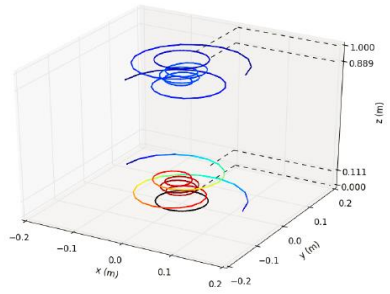

Figure 24 - Evolved solenoid antenna for WPT over multiple coils [39].

There are other methods to focus on the magnetic flux without any objects in the middle of the coils. In [40], the influence of a ferrite behind each coil is shown. Today, the major WPT system utilizes ferrite behind their coils. The magnetic properties of this material (high

permeability) lead to the focusing of the magnetic flux induced in each coil causing an increase in efficiency as shown in Figure 25.

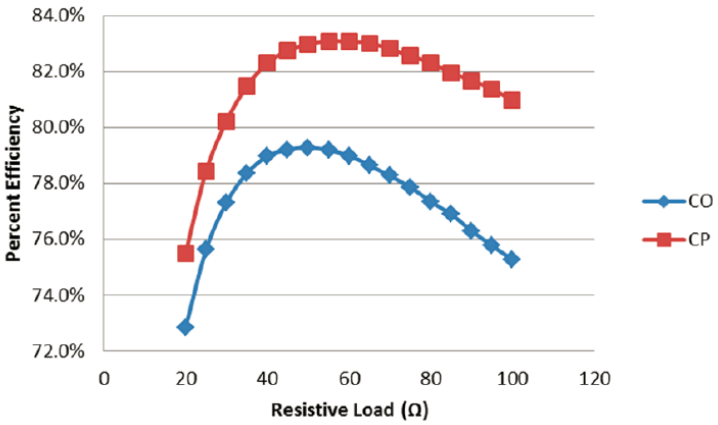

Figure 25 - Difference of a WPT system efficiency with and without ferrite behind the coils (CP) and (CO) respectively [40].

In [41], a method capable of maintaining high efficiency when the receiver coil is tilted is presented. By utilizing two lateral misaligned transmitters, as is demonstrated in Figure 26, when the receiver is tilted, one of the transmitters will have a higher coupling with it then the other, in order to maintain a high efficiency. In this way, the coupling between the transmitters and the receiver coils is still good enough to obtain overall high efficiency. However, the cost and size of the system will also increase.

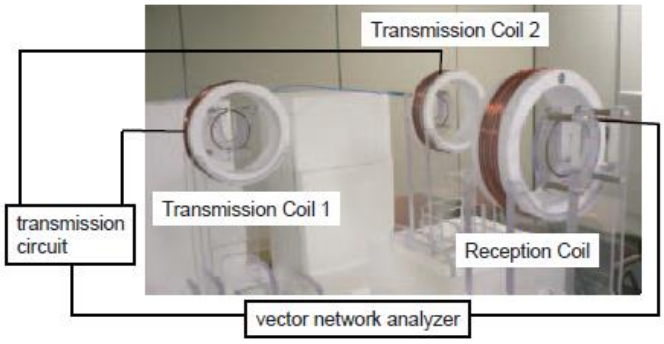

Figure 26 - Set up of the WPT system with two transmitter coils in [41]

2.3 Wireless communication

The most common wireless data transfer system for short range that also requires high data rates is Wi-Fi. In addition, other communication networks have also been used such as NFC and Bluetooth; however, they have much lower data rates than Wi-Fi. In [42], a system capable of transferring data at 875 Mbps by utilizing a 60 GHz wireless link called MMW (millimetre-wave) and a gigabit Ethernet communication is presented. Their system must operate in line-of-sight at the maximum distance of 10 m, which is not a disadvantage when considering the dissertation purpose. With 60 GHz (MMW), in [43], the importance of IEEE 802.15.3c which includes really high data transfer up to 1 Gbps is explained. This MMW offers a higher directivity when compared with Bluetooth and Wi-Fi that work at 2.4 GHz and 5 GHz. Different modulations were covered for several applications obtaining distinct data rates. 802.15 is an IEEE standard, which specifies wireless personal area network, with the 802.15.3 the standard for high rate. Within this group there are 802.15.3 a/b/c in which the velocity increases from a to c [44].

Commercially there are many available options for wireless communication, but only a few respect the principal requirements of the system. No module was found with 802.15.3c, which was the indicated communication protocol to include in the system's co-design. However, some of the smallest wireless data transfer modules found are presented below.

The Bluetooth V4.0 HM-11 is a module based on TI cc2541 chip that supports the specification V4.0 BLE. The module measures 13.5*18.5*2.3 mm^3 and features UART physical interface and is able to operate between -40 ºC and +65 ºC. The main characteristics of the module are its small dimensions, low power consumption and the supported Bluetooth specification V4.0 [45]. However, Bluetooth connections were made for low-speed data transmission (up to 1 Mb/s) and even when utilizing an advanced Bluetooth specification, it continues to not be enough for the LiDAR information [46].

Raspberry Pi Foundation is an UK company that provides low cost and high-performance computers, which allow people to solve problems by themselves. Their most recent product is the Raspberry Pi 3 Model B that can communicate wirelessly trough Wi-Fi and Bluetooth 4.1. Since the second generation of their products, all the modules support USB (UART), HDMI, Ethernet and SPI interface. The baud rate of all communication protocols has

increased version after version until it reached the Raspberry Pi 3 Model B. In this last one, the fastest and consequently more important communication interface is the BCM43438 wireless LAN (Wi-Fi) achieving the norm 802.11 n and the Ethernet with maximum throughput of 300 Mbps, with dimensions of 56*85*16 mm^3. The official temperature range is unknown. Recently they developed another third-generation kit called Raspberry Pi 3 Model B+ that can achieve Wi-Fi 802.11 ac for high baud rate communications as well as Ethernet with a maximum output of 300 Mbps.

ESP8266 is a low-cost Wi-Fi transceiver microchip with full TCP/IP stack and microcontroller capability. Several modules have risen with this chip since ESP-01 to ESP32. This chip allows connections to an 802.11 b/g/n network allowing high baud rate wireless communication. Different ESP modules were considered, but the one that met all the requirements was the ESP32 because it adds a physical ETH interface to the Wi-Fi connection. This opens the path for a quick and safe information transfer going from the LiDAR's sensor to the automobile. Espressif developed low-powered Wi-Fi and Bluetooth equipment by building a module known as ESP32, which features both Wi-Fi and Bluetooth for wireless communication and ETH 100 for wired communication. Compared to the previous one, this takes the advantage because the module with an U.FL male connector can be linked to an external antenna, keeping the actual module size of 18*19.2*0.8 mm^3. The operating temperature of the module is also accompanied by a temperature sensor with a range from -40 ºC to +125 ºC. To take advantage of all these specifications, a development kit which has the RJ45 connector for ethernet cable connection is used. The most appropriate devkit was the Olimex GATEWAY (Figure 27), due to its smaller size (51*62.5*16.2 mm^3), when compared to others ESP 32 devkits with the RF45 connector.

Figure 27 - Olimex GATEWAY board with the ESP32-WROOM-32U built-in.

The GSM150M is a low power Wi-Fi module with a U.FL connector for an external antenna establishing a connectivity 802.11 b/g/n. The module serial interfaces are SPI (with data rate up to 3 Mbps) and UART (with data rate up to 921.6 kbps) maintaining the absence of an Ethernet interface. The operating temperature is compatible with the automotive requirements (-40 ºC to +85 ºC). The module dimensions are 36.8*22.9*3.6 mm^3. The Wi-Fi connectivity could reach 72.2 Mbps but this velocity is limited when in Access Point mode as the ESP32 [47].

Comparing all the commercial options for a wireless communication module (represented in Table 4), it is possible to see that the better the data rate of interface and wireless communication, the bigger the modules. Since the data rate of both physical and wireless communication is of extreme importance, the raspberry Pi and Olimex boards were the most interesting, because they possess Ethernet with high data rates for physical communications and 802.11 n for high data rate wireless communications.

Table 4 - Comparison between the commercial Wireless communication modules.

Model	Communication	Size	Notes
Raspberry Pi 3Model B	Wi-Fi b/g/n Bluetooth 4.1 UART HDMI Ethernet 300 SPI	56*85*16 mm^3	It has a clock processor of 1.2 GHz and 1GB of RAM The most recent raspberry Pi 3 model B + could achieve Wi-Fi ac
Bluetooth V4.0 HM-11	Bluetooth 4.0 UART	13.5*18.5*2.3 mm^3	-
ESP32-WROOM-32U Olimex ESP32-GATEWAY	Wi-Fi b/g/n Bluetooth 4.1 UART Ethernet 100 SPI	Module: 18*19.2*0.8 mm^3 Devkit: 51*62.5*16.2 mm^3	The module has an U.FL connector to put an external antenna The Olimex devkit (ESP32-GATEWAY) has one ESP32-WROOM-32 module
GSM150M	Wi-Fi b/g/n UART SPI	36.8*22.9*3.6 mm^3	Does not support 802.11 n when it is in Access point mode

2.4 Co-design

There are some systems that embrace WPT and wireless communication in a single system with different techniques. In [48], both systems are presented using the same antenna with a dual resonant structure. They propose to include a bidirectional data transfer system using the WPT coil, both working with different frequencies. The coil size is 85*85 cm^2 and could reach 354 W and 19.2 kbps over 1 meter of distance between the coils, with a 51.977% power efficiency. In [49], a charging WPT and bidirectional data transmission system for traditional electric vehicles is proposed. Following Figure 28 Tx side (primary), it sends power to the Rx side (secondary) and data transmission occurs in both directions in order to establish a communication protocol. Like the previous system, this one also uses the same coils to communicate and to deliver power. They achieve the same efficiency of around 85% with and without data transfer, when the delivery power is between 400 W and 700 W.

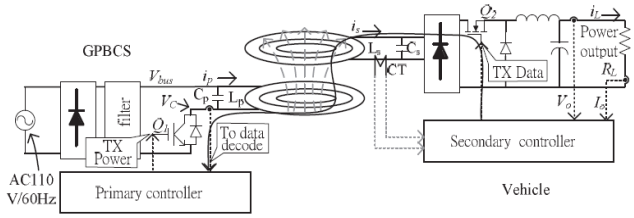

Figure 28 - WPT and wireless communication system of [49].

In [50], the impact of the WPT field in wireless communication is studied. Several techniques are studied to prevent the data transfer from being influenced by the wireless power transfer system like amplitude shifting, frequency shifting and phase shifting modulations. Their solution was to use different antennas for each system with different induced fields, magnetic (WPT) and electric (wireless communication). Their results proved that there is not a significant impact in power transfer at 20 kHz and wireless communication at 2.4 GHz. In [51], both single and dual frequency systems have been studied by implementing some design and circuit innovations.

Commercially, The Wireless Power & Communication target was the WPT market, illustrated in Figure 29. The 50W-HSD development kit offers a wireless transmission of 50 W across an air gap of 4 mm. In addition to the transmission of power, the development kit can also be used to communicate using Ethernet and RS232/485 that could reach 80 Mbps with ETH communication. However, the velocity of the wireless communication and the temperature range is unknown. It has a compact PCB design 90x35x32 mm^3 and a coil size of 58 mm of diameter [52].

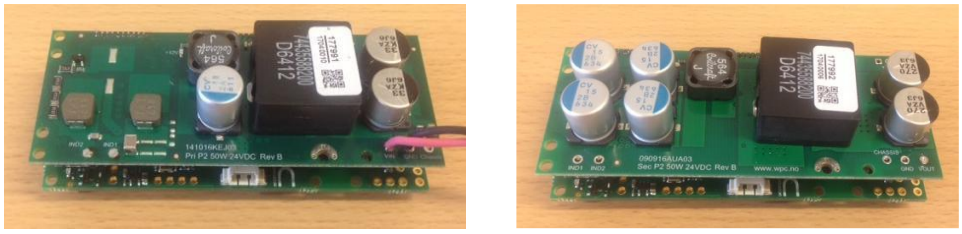

A B

Figure 29 - Transmitter side (A) and receiver side (B) [52].

Comparing this system with the ones presented in the last sections, this one is quite good since it can reach 50 W with small boards and it has Ethernet with a high data rate for communication. However, the wireless communication could not be compared because it is unknown.

CHAPTER 3 SYSTEM DESIGN

Considering that a power transfer distance around 10 mm OTA was requested, and that the efficiency was one of the principal requests for the system, the inductive coupling technique was selected as the one, which best fits the system requirements.

In this Chapter, some WPT coil simulations that will be made using the HFSS software, which run electromagnetic simulations, will be presented. This procedure will be carried out in order to better understand the best design that fits the system requirements, and obtain the coils with the highest coupling coefficient.

3.1 Simulations setup

By implementing a system with two coils, the Transmitter (Tx) coil and the Receiver (Rx) coil, the software, with an electromagnetic simulation, allows the user to gather some important aspects about the coils, such as the self-inductance, the mutual inductance between them and the information from the environment fields.

The software works with finite elements, requiring a good mesh to achieve the most correct results. The software provides an initial default mesh for any designed object, calculating its mesh with a defined parameter V, that represents the maximum length of each mesh element. This length is calculated by the software as an optimized value for correct and quick simulations. To study the initial mesh influence in the final values, different values of V will be utilized in order to obtain the results with different mesh refinements as shown in Figure 30.

The Solver setup will use several adaptive passes in order to warrant all the simulation requirements. In each pass an iterative algorithm solves the Electromagnetic fields of the model and refines the mesh. The setup will always take one pass after the other until the solution converges, or until the solution reaches the maximum of 10 passes (User-defined stop condition).

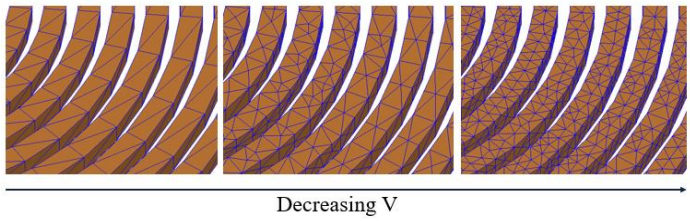

Figure 30 - Influence of decreasing the A in a coil mesh

An automatic adaptive meshing, which provides an accurate and efficient solution, has been used to eliminate the necessity for manual meshing expertise. This process will refine the mesh throughout the geometry by adding mesh elements in areas where a finer mesh is needed to accurately represent the electromagnetic behaviour of the model as shown in Figure 31. For that reason, a mesh refinement percent per pass of 30% was used. To prevent incidents where the solution does not converge, a maximum number of passes (10) has been defined. Regarding the reliable simulation results, 1% of error between passes seems to be a good compromise between time and quality of the results.

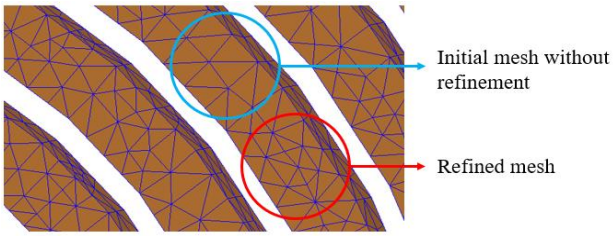

Figure 31 - Result of the adaptive mesh refinement

Before any numeric simulations can be carried out, a mesh study is required. After the coil simulations were concluded, new elements were inserted in the equation, requiring a mesh study of more than just the coils. To include all the utilized elements during the simulations, initial mesh study results for the coils, for the ferrite, for obstacles and for a shaft will be presented. The maximum length of each mesh element (V) is defined by default by the software, so a study is made by decreasing its value and comparing the result differences. In each mesh study, the variation of the coils self-inductance will be presented, but, the computation time, the energy error and the number of solver adaptive passes will also be shown.

To keep the results as precise as possible, different values of V were chosen to evaluate their influence in the system's inductances (L_T and L_R). Its final value will be selected, considering the relationship between more precise results and a reasonable computational time. The value of V of the coil's mesh was 1 for the ferrite, obstacles and shaft tests. For the tests of the obstacles and shaft, a ferrite in the design with the value of A of 1.5mm was also used.

In the tables bellow, some variables were used to understand the chosen values for the V. The s parameter represents the length of the coil's cross section side (1 mm). The f and h parameters represent the smaller size of the ferrite and the obstacles respectively (both 2mm). The r represents the shaft radius (2,5 mm).

Table 5 - Coil mesh refinement.

V [mm]	L_R [µH]	L_T [µH]	Simulation time [min]	Energy error (%)	solver passes
22,7 (default)	1,32	1,32	3	0,7	7
2 (2s)	1,31	1,31	6	0,6	3
1,5 (1,5s)	1,3	1,3	12	0,3	3
1 (1s)	1,29	1,29	14	0,6	2
0,75 (3/4s)	1,28	1,28	31	0,3	2
0,5 (s/2)	1,26	1,26	80	0,1	2

Table 6 -Ferrite mesh refinement.

V [mm]	L_R [µH]	L_T [µH]	Simulation time [min]	Energy error (%)	solver passes
6,8 (default)	2,27	2,26	16	0,8	5
4 (2f)	2,26	2,26	18	0,7	5
3 (1.5f)	2,27	2,26	17	0,8	4
2 (f)	2,26	2,25	20	0,6	4
1,5 (3/4f)	2,25	2,24	23	0,5	4
1 (f/2)	2,23	2,22	37	0,3	4

Table 7 - Solid Obstacle mesh refinement.

V [mm]	L_R [µH]	L_T [µH]	Simulation time [min]	Energy error (%)	solver passes
18,52 (default)	1,92	1,92	14	0,6	2
4 (2h)	1,92	1,92	16	0,6	2
3 (3/2h)	1,91	1,91	22	0,6	2
2 (h)	1,91	1,91	30	0,6	2
1,5 (3/4h)	1,9	1,9	50	0,5	2
1 (1/2h)	1,9	1,9	115	0,5	2

Table 8 - Sliced obstacle mesh refinement.

V [mm]	L_R [µH]	L_T [µH]	Simulation time [min]	Energy error (%)	solver passes
18,52 (default)	2,17	2,17	29	0,7	3
4 (2h)	2,17	2,17	20	0,7	2
3 (3/2h)	2,16	2,16	25	0,7	2
2 (h)	2,16	2,16	50	0,8	2
1,5 (3/4h)	2,15	2,15	58	0,8	2
1 (1/2h)	2,14	2,14	143	0,8	2

Table 9 - Shaft mesh refinement

V [mm]	L_R [µH]	L_T [µH]	Simulation time [min]	Energy error (%)	solver passes
8,02 (default)	4,25	4,25	95	2,95	10
8,02 (default)	5,50	5,50	14	2,04	6
5 (2r)	5,34	5,34	27	2,18	6
3,75 (1.5r)	5,29	5,29	35	2,24	6
2,5 (r)	5,28	5,28	37	2,41	6
1,875 (3/4r)	5.29	5.29	24	2,47	5
1,25 (r/2)	5,02	5,02	38	3,31	5

Relating to Tables 5 to 9, the coils' self-inductance tends to decrease with the mesh refinement, but the computational time mostly increases considerably in the final tests. With coarse mesh, the solver uses more passes until they converge and, in most cases, achieves less energy errors. However, in the shaft mesh refinement test, the solver could not find a convergence because the obtained minimum setup error was above 1%. A minimum setup error for the default value of V was reached in the sixth pass (2,04%) and this error increased until the tenth pass (2,95%), which leads to a worse solution with a higher computation time because with each pass the mesh becomes more refined. After this test the setup error was set to 2,5%. It was applied to all the resting values of V as well as for the default value. However, for the last two simulations, the setup did not converge again, so the setup error was changed again to 3% in the penultimate and last test respectively.

Taking into account that with coarse meshes the simulation already converges, for comparative tests simulations, the same mesh refinement will be used at all times in order to prioritize the simulation time and still have good comparative results. In this chapter the values used for V were s, f, h and 8,02 mm for the coil, ferrite, obstacles and shaft respectively.

3.2 Parametric analysis

Firstly, a two coils model was created in the HFSS software capable of simulating the inductance of the coils and their coupling coefficient. Considering a model with two coils, similar to a transformer, the primary coupling coefficient k1 is the proportion of the primary coils flux that links with the secondary, in the same way that the secondary coupling coefficient (k2) is proportional to the induced magnetic flux in the secondary that reaches the primary coil. By combining these two coefficients, the system coupling coefficient (k) is obtained:

$$k = \sqrt{k_1 k_2} \quad (3.1)$$

If both coils are close enough in such a way that all the magnetic flux from L_1 passes through L_2, k=1, the link efficiency is very high. If the distance between the coils starts to increase, part of the magnetic flux misses the receiver coil, decreasing the k and, consequently, the efficiency, until 0% is achieved for large distances [53].

To make a high-power system, this coefficient needs to be maximized. It is also necessary to have a high self-inductance of the Tx (L1) and Rx (L2) to ensure that all of the power is stored in the coils. For this, the term of mutual inductance (M) is introduced:

$$M = k\sqrt{L_1 L_2} \quad (3.2)$$

3.2.1 Modelling

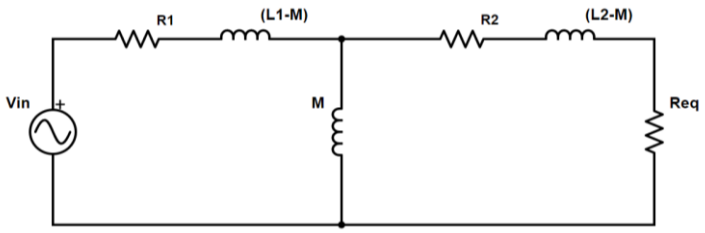

Figure 32 -Equivalent circuit of a WPT system.

Inductive coupling WPT systems are modelled using the conventional transformer model with an equivalent circuit as shown in Figure 32. The resistance R1 and R2 represent the resistance of the transmitter circuit and the receiver's circuit respectively.

To maximize the drop voltage in Req, it is necessary to maximize the M and minimize the (L1-M) and (L2-M). However, the most important part is to maximize the M in order to reduce the current that passes through it. The other two inductances will match the capacitors. Previously, the match between inductor and capacitors was mentioned. If capacitors that are in resonant with the coils (L1-M) and (L2-M) are used, the equivalent impedance is zero. Therefore, the circuit from Figure 32 is resumed in Figure 33:

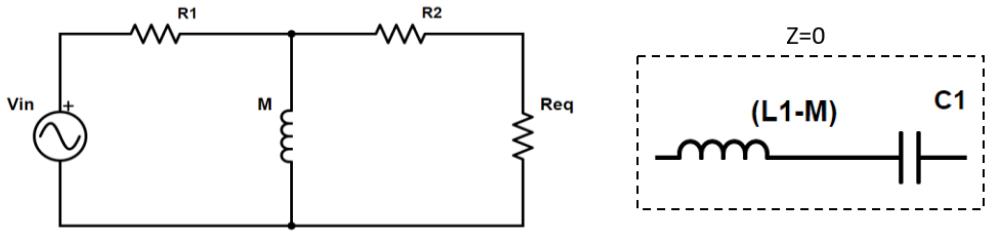

Figure 33 - Equivalent circuit of a WPT system with both coils in resonance with the system capacitors.

The remaining part of each resonate pair (coil plus capacitor), is the resistance R1 and R2. The R1 is the resistance part of (L1-M) and C1.

To help carry out the parametric analysis in HFSS, some variables were created, in order to study the impact of each variable in the system which are represented in Table 10. Tests were done in the software to obtain the best geometry to the WPT system including the final LiDAR's sensor. Each coil was supplied with an alternate current of 5 A. In order to test the behaviour of the system, the coils presented in Figure 34 were constructed following the values of Table 10. To test the impact of these variables, their influence in the mutual inductance will be tested. The coils have a square section due to computation time optimization. Coils with the same parameters were tested but with two types of cross sections: circular and square. After 3 different tests, both designs presented the same results but the circular one required computation times approximately 5 times higher.

Table 10 - Description and first value of the variable parameters.

	Variables	Value
H	Distance Between the coils	30 mm
Tx_rad	Tx section radius	0,5 mm
Tx_Rin	Inner radius of Tx	10 mm
Tx_sep	Tx gap between the turns	0,05 mm
Tx_turns	Tx number of turns	10
Tx_Rout	Tx out radius	20,45 mm
Rx_rad	Rx section radius	0,5 mm
Rx_Rin	Inner radius of Rx	5 mm
Rx_sep	Rx gap between the turns	0,05 mm
Rx_Turns	Rx number of turns	6
Tx_out	Rx out radius	11,25 mm

3.2.2 Influence of the distance between coils

By using a magnetostatics simulation, the coupling coefficient together with the mutual and self-inductance were calculated. Therefore, a comparison was made between the dependence of this parameter with the distance between the coils (H), as shown in Figure 34.

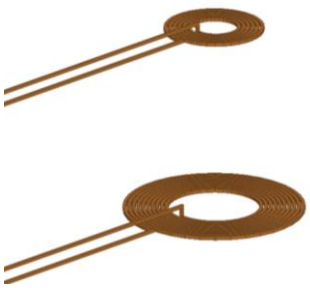

Figure 34 - Coil setup following

The obtained results, represented in Figure 35, confirm that for larger distances between coils, the mutual inductance decreases because fewer field lines of the magnetic field induced in the transmitter coil reach the receiver coil (decreasing k). Since the coil coupling coefficient (k) decreases, the mutual inductance also decreases since both are directly proportional.

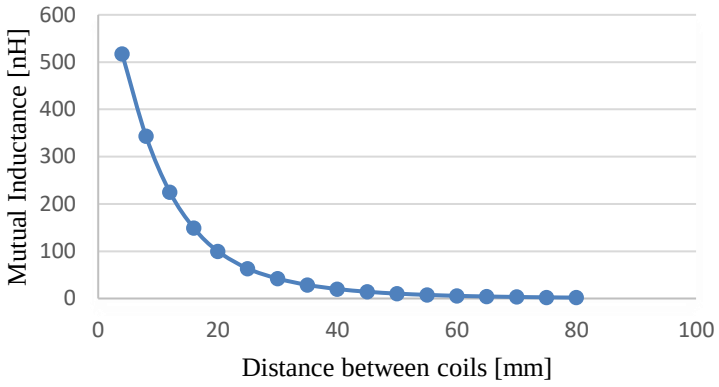

Figure 35 - Influence of the distance between coil in the mutual inductance.

3.2.3 Ferrite influence

Before evaluating all the influences of the parameters in Table 10 in the mutual inductance, a study will be carried out to determine the coil format that better enhances the magnetic flux through the coils. To improve the coils' coupling and impedance, four different cases of ferrite geometry (Figure 36) were compared.

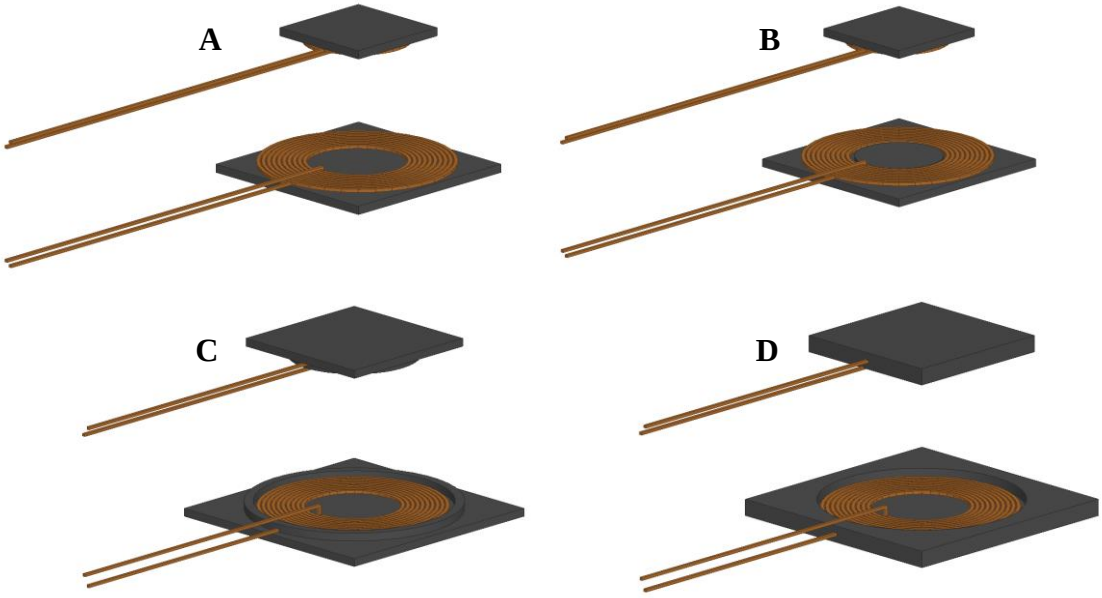

Figure 36 - Different designs of ferrites.

To compare the differences between the designs of Figure 36 and those of Figure 34, a simulation was run with the same variable values (Table 10). The obtained results of all the inductances and the coupling coefficients can be found in Table 11. The best ferrite design is design B as it has higher k and M values.

Table 11 - Comparison between the self-inductances, the mutual inductances and the coupling coefficient of the coils with all the ferrite designs tested above.

	L_R [µH]	M [nH]	L_T [µH]	k
Without Ferrite	0,73	20,03	3,75	0,0121
With Ferrite (A)	1,27	50,02	6,81	0,0170
With Ferrite (B)	1,36	55,80	7,14	0,0179
With Ferrite (C)	2,20	42,70	7,97	0,0102
With Ferrite (D)	3,15	39,97	9,01	0,0075

The differences between the first two designs is that in design B, an inner ferrite nucleus with a height equal to the wire's diameter was introduced. This approach considers this high as zero because it does not change the real coil distance, but if this value was increased beyond that limit, a new parameter called H_ferr would be considered. As its value increases, the separation between the coils decreases. Therefore, this parameter will be taken in account just from the end of the coil until the end of the nucleus, as shown in Figure 37.

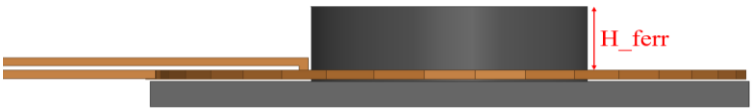

Figure 37 - Illustration of the design B with varying sizes of ferritic nucleus.

After selecting option (B) as the best ferrite option, it is time to check the influence of the H_ferr parameter. After some deliberation about the results presented in Table 12, it is perceptible that even with the withdrawal of the windings, the better result is when this parameter is maximum. Considering that the actual distance between coils remains the same (40 mm consistently), it can be said that the best design for the ferrite to obtain the maximum value of M is represented by the maximum size of H_ferr allowed, since it does not pass the

required size of the antenna, that could have at maximum height of 20 mm. Due to the fact that the ferrite base plus the copper wire measures 2.85 mm, the maximum H_ferr allowed is 17.15 mm.

Table 12 - Obtained results after testing different values of H_ferr

H_ferr [mm]	H [mm]	L_R [µH]	M [nH]	L_T [µH]	k
0	40	1,23	45,8	6,62	0,016
2,5	45	1,68	53,2	8,09	0,014
5	50	2,1	63,3	9,54	0,014
7,5	55	2,46	73,6	10,88	0,014
10	60	2,75	82,8	12,06	0,014
17,15	69,3	3,26	95,45	13,96	0,014

3.2.4 Inner radius influence

To obtain more realistic values compared with the final antenna size, the coils were made with a diameter of approximately 6 cm in order to match the actual maximum restrictions. To obtain such a size, the parameters have been changed to the values represented in Table 13.

Table 13 - New values for the variables.

Variables	Value
H	40 mm
Tx_rad	0,7 mm
Tx_Rin	10 mm
Tx_sep	0,1 mm
Tx_turns	13
Tx_Rout	29,4 mm
Rx_rad	0,7 mm
Rx_Rin	10 mm
Rx_sep	0,1 mm
Rx_Turns	13
Tx_out	29,4 mm

Next, with the 58,8 mm of diameter coils, some changes to the transmitter coil were made to understand the impact of the inner radius (Tx_Rin) and the turns of the coil (Tx_turns). To maintain the same coil size with the increasing inner radius, the number of turns must decrease as shown in Table 14. The tests will be done with H_ferr at zero.

Table 14 - Influence of Tx_Rin and Tx_Turns.

Tx_Rin [mm]	Tx_Turns	L_R [µH]	M [µH]	L_T [µH]	k
4	17	12,80	1,29	14,26	0,0951
7	15	12,81	1,28	13,82	0,0962
10	13	12,81	1,25	12,83	0,0975
13	11	12,82	1,18	11,25	0,0986

With these results, it is possible to conclude that decreasing the radius and increasing the number of turns produces better results, even though the ferrite nucleus has decreased its size. Therefore, the size must be the smallest possible, bearing in mind the application restrictions about the inner size.

3.2.5 Winding separation influence

To study the influence of the separation between turns of the coil (Tx_sep), the same principle of the previous test perpetuates, so the Tx_Rin was also changed to keep the coil size the same. To meet this end, when the separation between turns of the Tx is increased, its inner radius must also decrease. Regarding Table 15, it can be seen that the dependence of the Tx_sep was not very significant. Even though the use of Tx_sep of 0.1 mm still achieves better results, which is in accordance with the previous test, the best results were obtained with the smaller inner radius.

Table 15 - Influence of Tx_sep.

Tx_Rin[mm]	Tx_sep[mm]	L_R [µH]	M[µH]	L_T [µH]	k
10	0,1	12,812	1,250	12,828	0,0975
10,6	0,05	12,373	1,125	12,878	0,0891

The dependence of the wire section was not studied because its value must be high enough to conduct the current. As the final system will be high powered, a section capable of conducting a maximum of 10 A was selected. If necessary, this section might be switched.

3.2.6 Lateral and angular misalignments influence

The influence of the coils lateral and angular misalignments was also studied. These misalignments are represented in Figure 38.

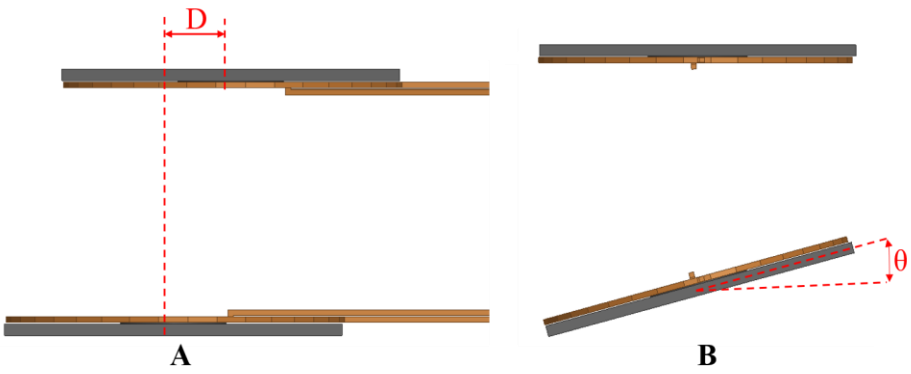

Figure 38 - Lateral (A) and Angular (B) misalignments of the coils.

With these two tests, it is possible to obtain the response of the system to slight misalignments that may occur temporarily. With these analyses it is possible to conclude that the impact of both misalignments is very passive when compared to the one registered in the distance between coils. The influence of small angular misalignments (Figure 40) is practically negligible when compared to the influence of lateral misalignments (Figure 39) or even the distance between coils. The angular misalignment behaviour could be explained by the fact that the rotation axis is in the middle of the coil, since one part of the coil will be farther away and the other, closer to the receiver coil in the same proportion, keeping the mutual inductance approximately constant as shown in Figure 40.

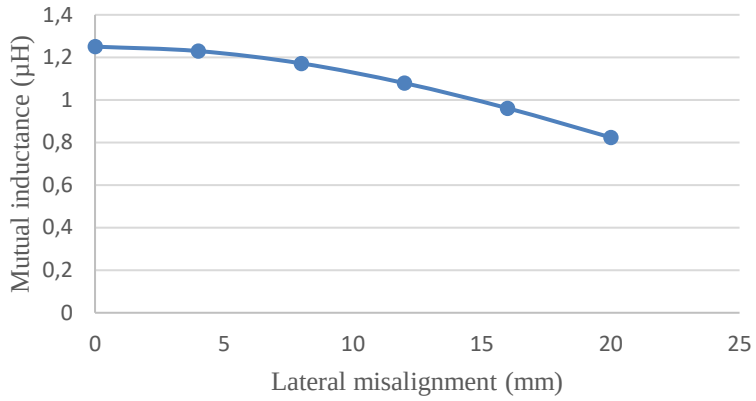

Figure 39 - Lateral misalignment dependency on M

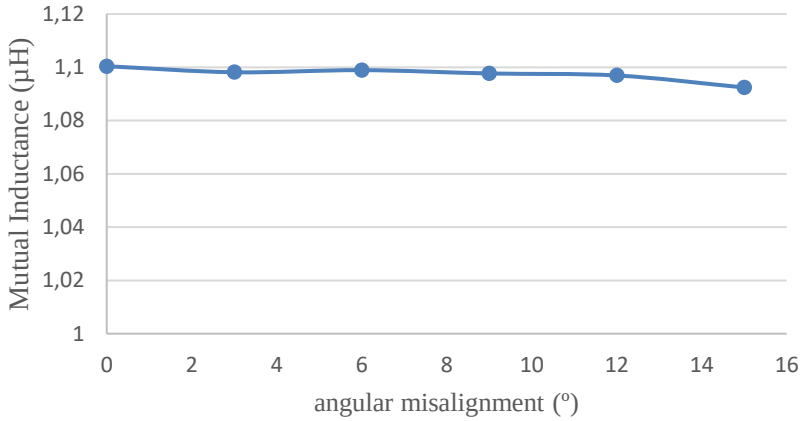

Figure 40 - Angular misalignment dependency on M

3.3 LiDAR's sensor setup

Considering that the WPT system will power a rotate LiDAR, there is a necessity to find a mechanism to make it rotate. That mechanism could be out of the WPT system or could be achieved by placing a shaft in the middle of both coils. Considering the second method, the shaft's magnetic properties could be used to improve the system mutual inductance as well as the coils' self-inductance. Considering the ferrite purpose, a nucleus that enhances the coils' coupling coefficient is also viable.

3.3.1 The shaft material

The nucleus can be made of many materials and by implementing a shaft between the coils as shown in Figure 41, it is possible to predict what the magnetic behaviour of the system would be with such a mechanism.

For this purpose, it is expected to make use of a material with a high permeability, low conductivity and enough stiffness to support the LiDAR system on it. Considering the values of Table 16, the ferrite is the first choice for the shaft material however; the mechanical properties of the ferrite are not adequate to support a system on it. Therefore, studying other materials needs to be set as a priority.

Table 16 - Relative magnetic permeability and conductivity of some materials.

Material	Relative magnetic permeability (μ)	Conductivity (Siemens/m)
Air	1	0
Ferrite	1000	0,01
Iron	4000	10300000
Aluminium	1	38000000

Values with no nucleus (air) were compared with the best material for the job (ferrite) with a typical shaft material (aluminium) and with a suggestion for a shaft with optimal magnetic properties (iron). First, and for a coil inner radius of 10 mm, a nucleus of 9.1 mm of radius was utilised, simply for testing purposes, as shown in Figure 41.

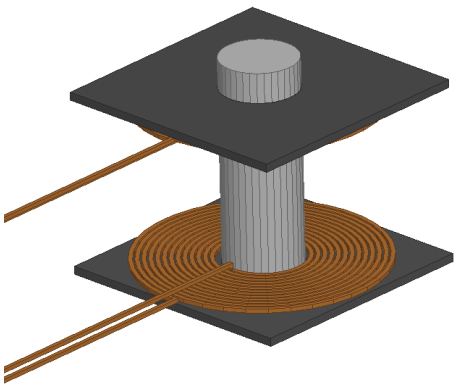

Figure 41 - Shaft between the coils.

Table 17 - Influence of the material's shaft.

Material	L_R [µH]	M [µH]	L_T [µH]	k
Air	11,60	0,98	11,60	0,084
Ferrite	38,94	22,16	38,95	0,569
Iron	39,57	22,69	39,58	0,573
Aluminium	11,58	0,98	11,59	0,084

The test was made in the same conditions as the previous ones. Considering

Table 17, the results with the higher permeability have much higher mutual inductance with the iron and ferrite shafts representing the best results. Each of them obtains a mutual inductance even higher than each coil's self-inductance while compared to the system with an aluminium shaft or without a shaft (air). However, this simulation does not include the core losses and iron which will have high values due to its high conductivity. Aluminium also has this high conductivity, but it does not heat too much because it doesn't enhance the magnetic flux as much as iron. The high magnetic flux inside the iron shaft will induce eddy currents and the losses will occur by Joule's law. Even so, it is still an option to utilize an iron shaft since the eddy currents were extremely reduced by laminating the material's core, due to the fact that the eddy currents will only flow separately in each plate as is shown in Figure 42. This technique is commonly used in the transformers' cores to minimize the core losses obtaining higher efficiencies. For the WPT ensemble, where the frequencies are commonly higher, the inducted eddy currents are even stronger due to the higher magnetic flux that pass in the material, so, it is of extreme importance to minimize them.

Laminating the shaft could be an optimal solution to reduce the shaft losses and to keep a high coupling between the coils.

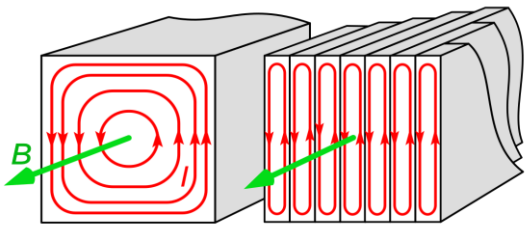

Figure 42 - Lamination effect in eddy currents [54].

3.3.2 Coils' quality factor

Considering a typical shaft size (4 mm of diameter), the rest of the system can be reduced. To obtain the same mutual inductance as in the design without the shaft, the Rx and Tx systems were reduced by changing the Inner radius to 2,7 mm and the number of turns to 8 in both coils, resulting in a final size of approximately 3*3 cm^2. The presence of a nucleus provides higher chances of minimizing the size of the final system.

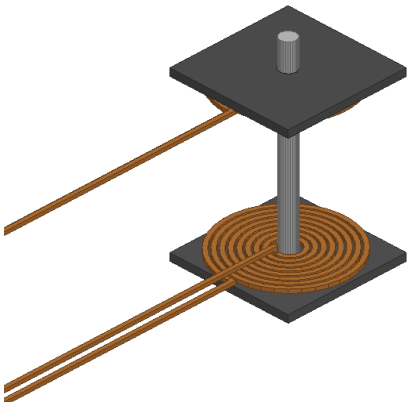

Figure 43 - Reduced system with a 4mm shaft.

With the design represented in Figure 43, the influence of the frequency was measured (represented in Table 18).

Table 18 - Influence of the frequency.

F [MHz]	L_R [µH]	M[µH]	L_T [µH]	ZL_T[Ω]	ZL_R[Ω]	ZM[Ω]
0,5	11,98	1,06	11,99	0,146 + 37,64i	0,145 + 37,67i	0,012 + 3,33i
1,0	11,98	1,06	11,99	0,148 + 75,25i	0,146 + 75,31i	0,012 + 6,66i
10,0	11,98	1,06	11,99	0,149 + 752,46i	0,147 + 753,07i	0,012 + 66,63i

The power that a coil can transfer can be modelled by the following expression:

$$P = |Z|I^2 \quad (3.3)$$

|Z| is the module of the complex number shown in the Table presented above. The impedance of the coil (Z) is separated in an imaginary and a real part. The real part represents the resistance of the coil, which is responsible for the dissipated power in the coil. As the imaginary part of the Z is the impedance of an ideal coil (ωL), the Im[Z] is directly proportional to the frequency. So, for higher values of |Z| and for the same power, the current needed to flow through the coil is smaller. This implies a higher quality factor of the coil once the real part of Z remains constant with the changes of frequency.

The coil's quality factor is a decisive point when selecting the coil, due to the relationship between the imaginary and real part of Z. Therefore, through the comparison of this factor at the same frequency between several coils, it is possible to point out the coils that will heat due to its resistance.

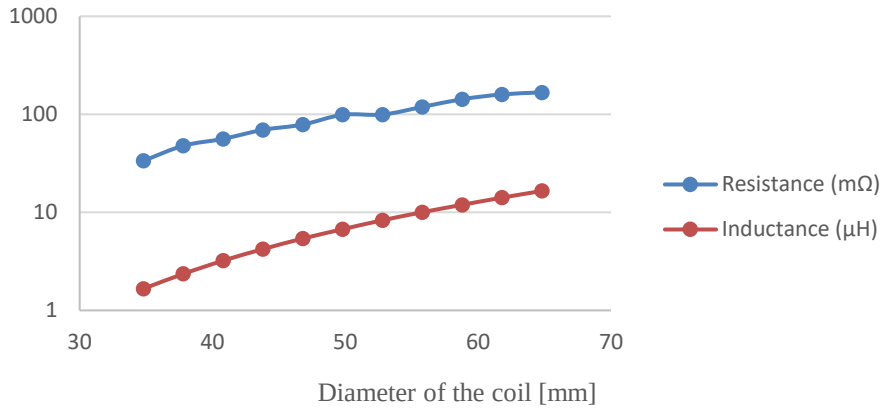

Figure 44- Influence of the coil's size in the resistance and self-inductance.

To see the influence of the coil's size in the inductance and resistance, the number of turns of the coil was increased and consequently the amount of copper too. So, an increase in the resistance was expected such as the inductance of the coil as demonstrated in Figure 44. Taking into account the logarithmic scale utilized, it can be seen that the quality factor increases with the coil's size too.

3.3.3 Multilayer coils

Regarding the utilization of a shaft, the coil's format optimization to adapt to this new design could be important. The first approach was to get the coil closer to the shaft to induct a higher magnetic flux inside of it. For that, coils with more than one layer were created. The idea was a tall and narrow coil with less turns but more layers, with the intention of getting each winding closer to the shaft when compared with the flat option (1 layer) as suggested in Figure 45.

Regarding the size requisites, the height of the coil plus the ferrite could not surpass 20 mm. 2, 5 and 9 layers with different turns were tested with the intuit of determining the best layout. In Figure 45, the 9 layer layout is illustrated with the same parameters as before except for the number of turns, which for these tests is only four and the distance between coils that is 15 mm.

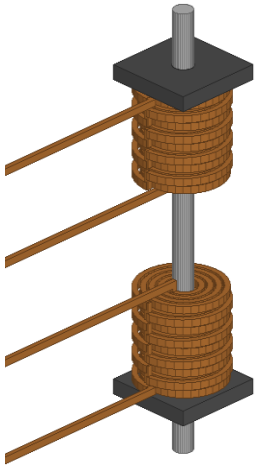

Figure 45 - 9 layers' design

As predicted and through the analysis of Figure 46, with the use of a nucleus, the options with more than one layer could achieve much higher inductances. The one that presented the best results was the coil with 5 layers, which has higher mutual inductance and self-inductance than all the others from 50 µH forward for the same coil resistance. However, for lower values of inductance (less than 50 µH) almost all the designs have the same resistance, which allows

some liberty to design the final coils of the system. Since the WPT system needs to be built-in with other systems in the LiDAR sensor, the possibility of changing the design of the WPT without compromising the efficiency is always an advantage.

With a multi-layer design, it was possible to obtain a much higher mutual inductance respecting the space requests, due to the fact that much higher self-inductances are achieved when compared with the "1 layer" design (Figure 43).

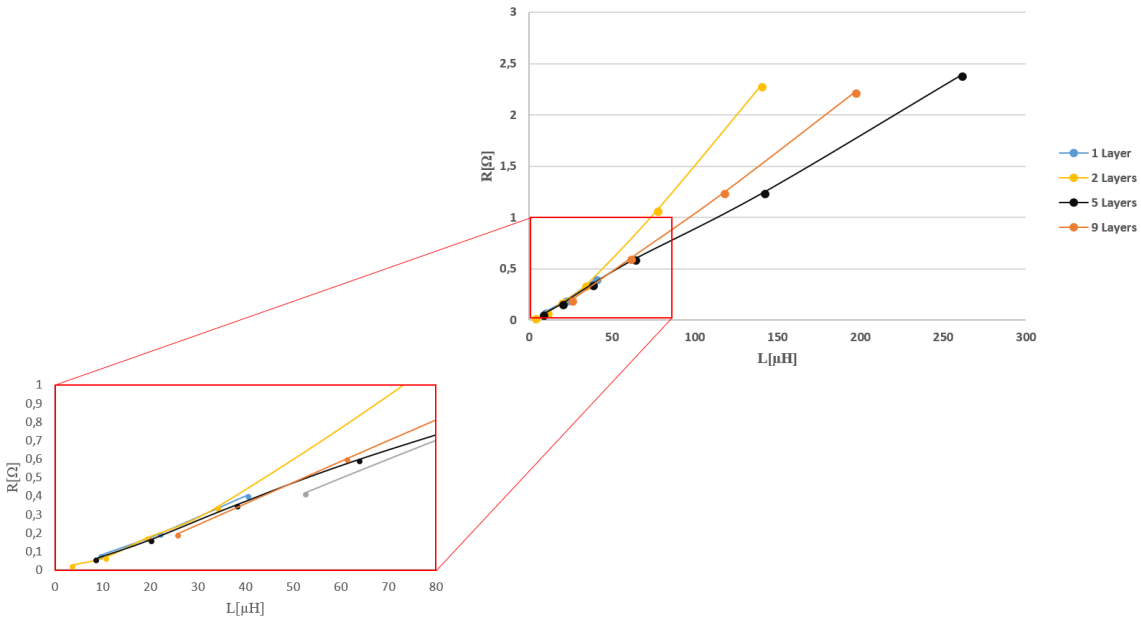

Figure 46 - Relation of self-inductance and resistance of the coils with the number of layers influence.

3.3.4 Interference caused by obstacles

As previously mentioned, the WPT system will be incorporated in a LiDAR sensor, which implies that the magnetic flux field should not suffer interference from those systems. Some metallic parts need to be considered too. As denoted through the shaft material tests, some materials, in close proximity to the WPT, could lead to several changes in the coils' coupling. To study some possible metallic objects between the coils or immediately above one coil, objects with dimensions of 88*88*2 mm^3 will be used. This experiment serves the purpose

of comparing the behaviours of such objects when they are massive or sliced (Figure 47). These sliced parts will be replaced by a polymer.

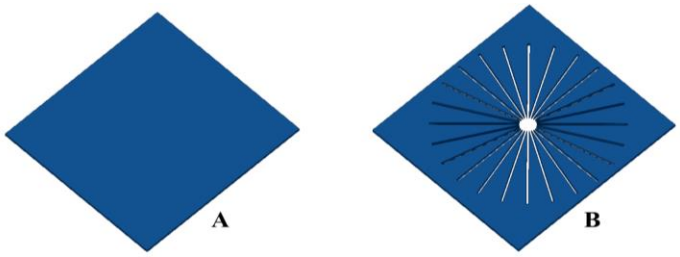

Figure 47 - Tested massive (A) and sliced (B) obstacles.

The obstacles of Figure 47 will be placed between the coils or above the Rx coil to predict the behaviour of the system when facing such situations by being placed inside the LiDAR's sensor. The results presented in Table 19 follow the values shown in Table 20. The tests were made without any shaft and with flat ferrite plates behind the coils following the design A of Figure 36.

Table 19 - Influence of obstacles in the coil's coupling.

	L_R [µH]	**M [nH]**	**L_T [µH]**
Air	2,25	47,16	2,24
Middle massive iron	2,31	4,08	2,32
Middle sliced iron	2,30	5,17	2,31
Above massive iron	2,26	60,74	2,37
Above sliced iron	2,25	60,19	2,36
Middle massive aluminium	2,21	0,10	2,18
Middle sliced aluminium	2,23	34,42	2,22
Above massive aluminium	2,25	33,63	2,18
Above sliced aluminium	2,26	40,59	2,22

The results observed in Table 19 suggest that a massive block of aluminium or iron in the middle of the path interrupts the connection between the coils. However, when that block is sliced something different happens, because with the results obtained, the situation with the aluminium block gets closer to the situation without obstacles (air), while the process of slicing the iron block does not affect the system's behaviour. This difference could be explained by the

strong magnetic permeability of iron, which locks up the magnetic flux closer to it, even when it is sliced. Even so, the aluminium, when sliced, has less eddy currents induced and more "open" space to let the flux pass to the other coil. With the obstacles out of the fields' path (above the Rx coil), the magnetic field assume a new behaviour. Both the massive and sliced block of iron has identical behaviours enhancing the mutual inductance to higher values than without any obstacle. However, thanks to its magnetic properties, the block will heat as an inductive field cooker heats a pan and even with the sliced block, it is expected to find a lot of heating in the iron plate. When the aluminium block is above the receiver coil, an acceptable mutual inductance between the coils, which is higher for the sliced block, still exists, as expected because it has less eddy currents induced, resulting in fewer losses.

Table 20 - New values for the variables.

Variables	Value
H	40 mm
Tx_rad	0,7 mm
Tx_Rin	5 mm
Tx_sep	0,1 mm
Tx_turns	8
Tx_Rout	16,9 mm
Rx_rad	0,7 mm
Rx_Rin	5 mm
Rx_sep	0,1 mm
Rx_Turns	8
Tx_out	16,9 mm

CHAPTER 4 SYSTEMS CO-DESIGN AND TESTING

In this chapter, two WPT systems and one wireless communication system will be presented and tested. The wireless power tests will be made as a function of the efficiency instead of the mutual inductance as in the previous chapter. In order to achieve the most precise results, a relationship between the efficiency and the mutual inductance will be established. The final setup, which contemplates the co-design of both wireless systems, will be presented too.

4.1 Wireless power system

In the last chapter, the equivalent circuit of two coils was presented. Therefore, another path of interpretation of the circuit will be followed in order to obtain its efficiency. Considering a power supply (V) capable of introducing a current I in the circuit of Figure 48, it is possible to obtain the equation (4.1) following Kirchhoff's law.

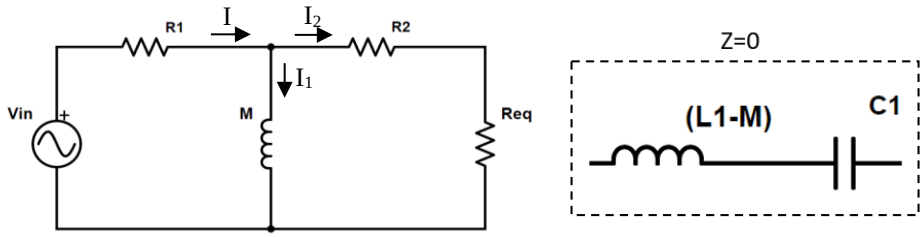

Figure 48 - Equivalent circuit of a WPT system with both coils in resonance with the system capacitors.

This current will be divided through the M path and the R_{eq} path corresponding to:

$$I = I_1 + I_2 \quad (4.1)$$

Like the aforementioned law proposes, the voltage drop at the coil terminal is:

$$V_1 = V - V_{R1} \quad (4.2)$$

where (V_{R1}) the voltage drop is in the resistance R_1. Consequently, the coil (M) current is calculated by the following expression:

$$I_1 = \frac{1}{M} \int V_1 \, dt \quad (4.3)$$

Using Kirchhoff's law, the voltage drop in the R_{eq} is:

$$V_2 = V_1 - V_{R2} \quad (4.4)$$

According to the ohms law, R_{eq} is presented in the following expression:

$$R_{eq} = \frac{V_2}{I_2} = \frac{V - V_{R1} - V_{R2}}{I - \frac{1}{M} \int (V - V_{R1}) \, dt} \quad (4.5)$$

Assuming all previous equations, it is possible to obtain the efficiency of the system:

$$\eta = \frac{V \, I}{V_2 \, I_2} = \frac{V \, I}{(V - V_{R1} - V_{R2}) \, (I - \frac{1}{M} \int (V - V_{R1}) dt)} \quad (4.6)$$

Looking at the previous expression, the power supply losses are the voltage drop in resistance 1 and 2, which needs to be minimized, and a M that needs to be maximized. There is another way that is not directly seen in the last formula. The frequency will not affect the value of V_{R1} and V_{R2}. The impact of the increase in frequency is much greater in the current that flows through the coil M, by proportionally increased impedance, which will have much less current through it and consequently the I_2 will be higher (higher efficiency). However, when the mutual inductance is high enough for a good coupling efficiency, it is not necessary to increase the frequency because problems such as parasitic capacitances and parasitic resistance could be encountered when the system operates at radio frequencies (RF).

4.1.1 Transmitter and receiver modules

After considering all the available options in Chapter 2, the Würth Elektroniks WPT system was recognized as the one that best met all the requirements. It has a small board and the option of easily changing some components to fit the automobile requirements or improving the efficiency for the specific final design. The company provided the Eagle files of the board and schematic. From these files the bill of material (BOM), and the Gerber files to print the PCB were obtained.

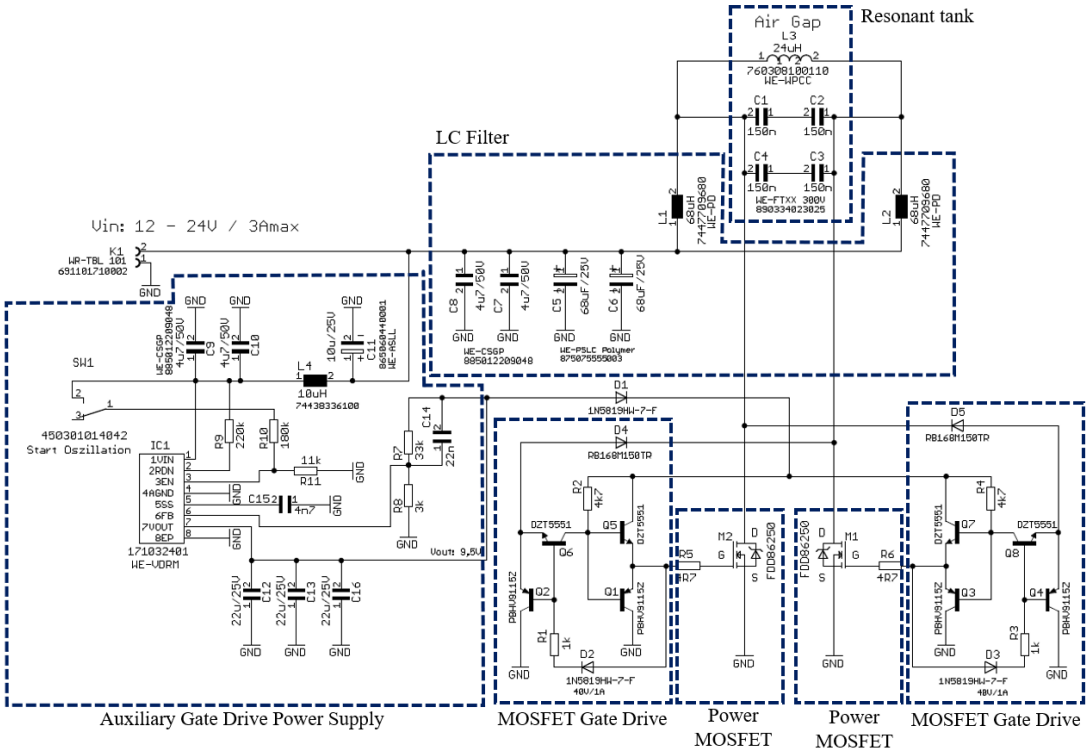

Figure 49 – Würth Elektroniks transceiver (schematic adapted from [55]).

Taking into account the schematic presented in Figure 49, the power transfer coil (L_3) has an inductance of 24 µH and a quality factor of 180 at 125 kHz. Such power transfer coil was swapped for another with the inductance of 19.5 µH and quality factor of 220 at 125 kHz. The suggested coil inductance would be very affected if the shaft scenario came true, due to the fact that it possesses a middle magnetic nucleus above the ferrite and in the middle of the inner coil winding. The replacement suggestion only has the ferrite enhancing its magnetic flux, so it

will be easier to use in a shaft design by simply making a hole in the ferrite. Even with this change, it is predicted that the system maintains the same behaviour. Both transmitter and receiver will have the same schematic and will work differently depending on which role they interpret.

In Figure 49, the schematic of the transmitter and receiver module is presented. The Tx's operating principle is of an oscillator that will receive a DC and convert it to an AC with the resonant frequency between the WPT coil (L3) and the connected capacitors (C1/C2/C3/C4). These components built a LC resonant tank, in which the frequency could vary depending on the coil's inductance value. The distance between the coils will affect the self-inductance of each one of them due to the fact that the proximity between coils will imply the proximity of the ferrite of one coil to the other coil. Therefore, when the coils come closer, both L_T and L_R will increase and therefore involve a lower resonant frequency.

The MOSFET gate drives control the power MOSFET through push-pull switching of the gates. When the circuit is powered, one of the MOSFETs starts to conduct a fraction of second earlier than the other and, from then on, they start to work out of phase as Figure 50 suggests. In this Figure, the signal of each MOSFET gate, measured in an oscilloscope is presented. Each MOSFET will then conduct in half the period of the transmitted magnetic field. The opposition of phase is controlled by the MOSFET gate drives and, the frequency will be defined by the resonant tank. When the MOSFET M1 starts to work in the linear region and M2 starts to work in the cut off region, the right side of the resonant tank is forced to maintain the ground potential, while the other side is charging and discharging the resonant tank as Figure 51 demonstrates. When the voltage drop at the resonant tank is zero, the MOSFET gate drive circuit will force the MOSFETs to switch their state. In summary, M1 starts to work in the cut off region while M2 starts to work in the linear region and the exact behaviour repeats in opposite sides of the resonant tank.

This oscillating behaviour will only exist when the SW1 is closed and the Vin is high enough to power the IC1. When all that is accomplished, the auxiliary gate drive power supply will deliver energy to the MOSFET gate drive.

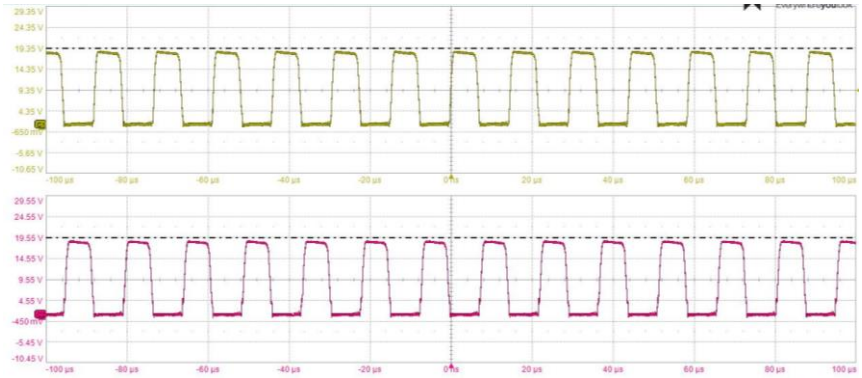

Figure 50 - Voltage signal in the MOSFETs gate, relatively to the board ground, measured in the oscilloscope.

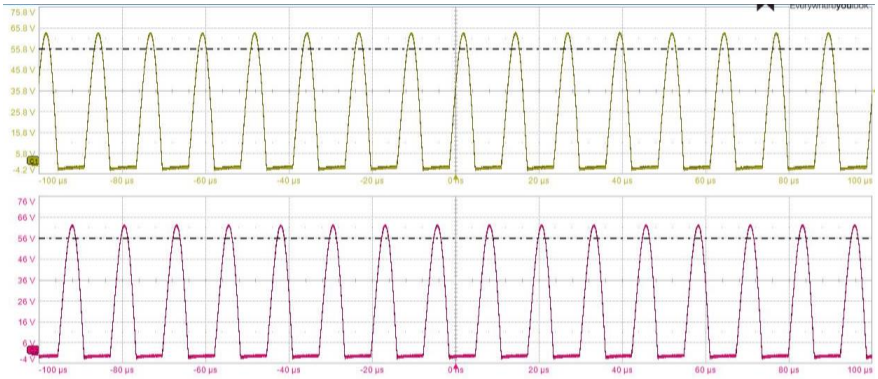

Figure 51 - Voltage signal in each coil terminal, relatively to the board ground, measured in the oscilloscope.

When the circuit of Figure 49 works as a receiver there are many differences. The receiver works with SW1 opened or closed and the IC1 is not necessary, resulting in the simplified circuit of Figure 52. Consequently, the MOSFET gate drive power supply will not supply the MOSFET gate drive, which in turn will make the MOSFET gate drive and MOSFET power work differently. When the AC wave reaches the resonant tank, these two MOSFET circuits will rectify the signals of both sides of the resonant tank, in opposition of phase, forcing the wave form in the receiver as illustrated in Figure 51.

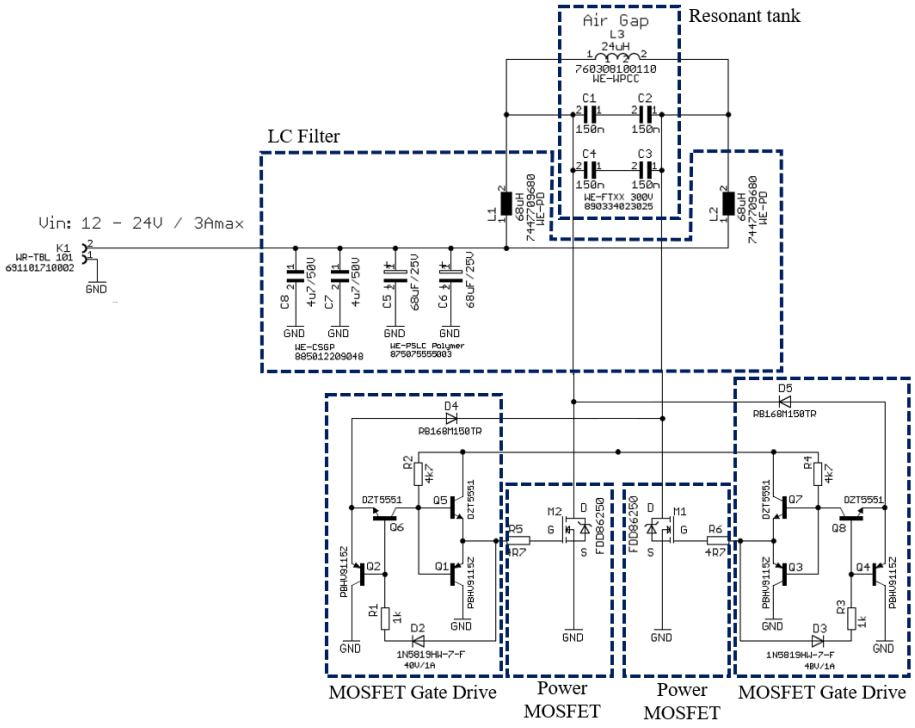

Figure 52 - Simplified receiver circuit (schematic adapted from [55]).

As both receiver and transmitter resonant tanks are equal, the wave form that reaches the Rx coil is equal to the one that is in the transmitter coil (Figure 51), with the difference of the amplitude because not all the energy passes to the receiver board. It is expected that the frequency of the wave stays the same as both resonant circuits are equal. Some of the power is lost through the coupling inductance that exists between the coils and by resistive losses of the module's circuit. Therefore, the signal amplitude is also represented in Figure 51, but that amplitude will depend on the distance between coils. The mutual inductance will decrease with the increasing separation between coils, which implies that a signal with lower amplitude will reach the receiver.

A LC filter is usually applied to a full rectified wave in order to obtain a DC output. However, the signal that reaches each side of the tank is only half rectified (as Figure 51 suggests). By applying one coil to each half-rectified wave and connecting both coils' terminals, it is possible to have the same behaviour as with one coil after a full wave is rectified. The capacitors complete the LC filter to have a constant signal in the terminal block K1.

With the eagle files given by the company, the Gerber files were generated in order to print the PCBs. Taking into account that both boards have the same circuit. One of the two printed boards is represented in Figure 53.

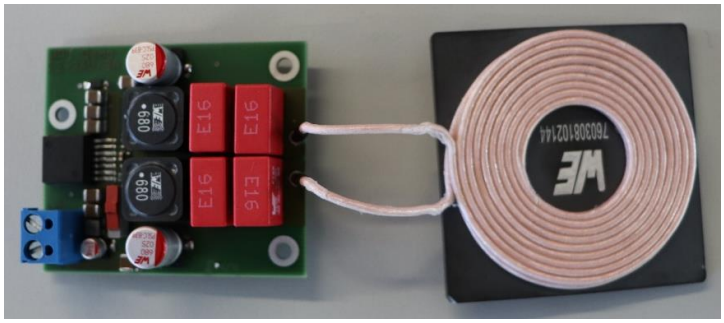

Figure 53 - Würth Elektroniks printed board.

A third-party company was asked to create a prototype with the purpose of meeting the requirements presented in Chapter 1. Due to the NDA conditions, from this point onwards, this company will be referred as "company A". To preserve all their technology, they sealed the modules just for test purposes. The size of the transmitter module is 100*60*40 mm^3, and the receiver module is 100*40*20 mm^3. Both of the coils have dimensions of 85*85 mm^2. They guarantee their product will have a maximum efficiency of 55% over an air gap of 8,5 mm between coils. The agreement allows for the system to be kept during a short period of time, however, the co-design test cannot be done because the communication system was not ready at the time.

The housing of the WPT system is also an important topic that needs to be reviewed. This protection will be of extreme importance for future EMC measurements. However, without all the LiDAR's sensors finished, the housing has not been built yet. In future work, some attention will be given to this important factor.

4.1.2 Results

Regarding the presented Würth Elektronik WPT and the "company A" WPT systems, some of the tests performed in the simulations will be reproduced. Considering the known aspects about the two systems, and that not all the tests made in the simulations can be performed, only the influence of distance, misalignments between coils and the presence of obstacles on the efficiency will be tested.

As before mentioned the mutual inductance is proportional to the efficiency. The simulations show the results as a function of the mutual inductance and the real systems' tests will be made as a function of the efficiency.

The Würth Elektronik system has an oscillator circuit which frequency varies according to the resonance frequency of the resonance tank. Thus, the circuit will always be optimized for every tested setup. However, the "company A" system works only at a fixed frequency. In this way, any test that removes the system from its ideal position (8,5 mm between coils which are laterally and angularly aligned), will introduce a mismatch in the resonant tank, which will store part of the transmitted energy.

To achieve the desirable power in the load for the "company A" system, 4 resistors of 4 Ω and 10 W each were used since the maximum power the system could provide is approximately 40 W at the optimal distance 8,5 mm. The resistors were dimensioned so all the power available in the receiver module (12 V and 3,3 A) can be delivered to them. Ideally the resistance value should be 3,6 Ω and 40 W, however, the closest possible available resistances were of 4 Ω and 10 W each. By placing two serial resistors in parallel with another two, the resulting resisting will still be 4 Ω but the power will now be 40 W. To deliver power to a load using the Würth system, two resistors of 22 Ω and 25 W each will be utilised. They will be placed in parallel to obtain an equivalent resistor of 11 Ω and 50W.

Figure 54 – "Company A" system testing setup.

In Figure 54, the setup made for the "company A" system tests is represented. The Würth tests were also made using this setup which has an arm with a vertical regulable support where the Rx coil of both systems was placed during the tests. The support also allows the accomplishment of the angular misalignments by changing the support inclination as suggested in Figure 55. Tests of the distance between coils, angular and lateral misalignments and the presence of massive obstacles between coils and behind one coil, have been performed. These tests will be presented as a function of the whole system's efficiency.

Figure 55 - Angular misalignments setup.

The Figure 56 represents both systems' efficiency depending on the distance between coils. The Würth system achieves much better results, with a maximum efficiency of 81%, while the "company A" system can only achieve a maximum of 54%. Observing this Figure, it is possible to see that in the first 15mm between coils, the Würth system maintains approximately the same efficiency so the value of the mutual inductance is high enough to maximize the coils' coupling efficiency. In these first millimetres, it is expected that the only losses are due to the boards and coils resistance since the resonant frequency is kept in these lower distances. However, the "company A" system always operates at the same frequency, and the maximum power delivered to the load is obtained only at 8,5 mm between the coils, even if the efficiency is higher for smaller distances, which meets the results of the simulations.

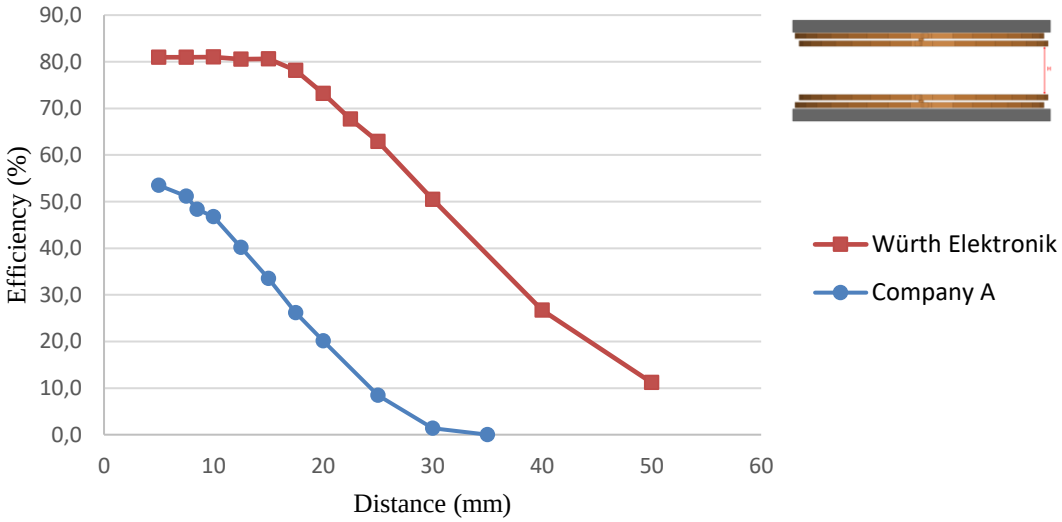

Figure 56 - Distance between coils influence in the efficiency of the WPT systems.

Similarly to what happens in the angular and lateral misalignments, a simulation in the previous chapter, the obtained results for the real system continues to maintain the same behaviour with the efficiency presenting the same qualitative results as the mutual inductance obtained in the simulations. In Figure 57, both systems' efficiency when the receiver coil is tilted is represented, and in Figure 58 the efficiency of both, when the coils are laterally out of alignment is also represented. For these tests, the distance between coils were 21 mm for the Würth system and 30 mm for the "company A" system, but in the lateral misalignment of the

"company A" system the separation between coils was 8.5 mm. It is possible to conclude, that even with the ferrite used in the Würth system, the results obtained in the misalignments were qualitatively similar in both systems. The obtained low values from the "company A" system can be justified due to the large WPT coils, which need to be 30 mm apart to allow a maximum 35 º tilt angle, as illustrated in Figure 55.

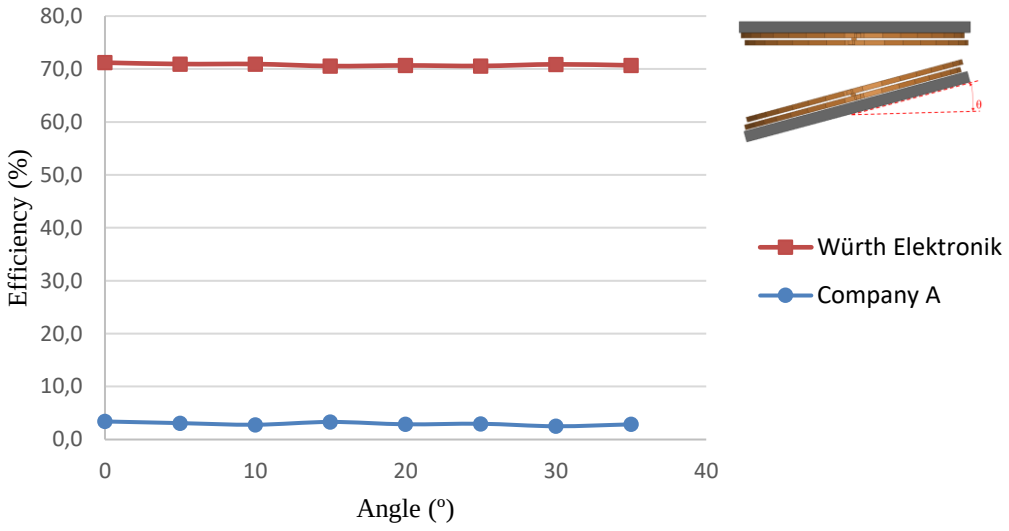

Figure 57 - Influence of the angular misalignments in the efficiency of the WPT systems.

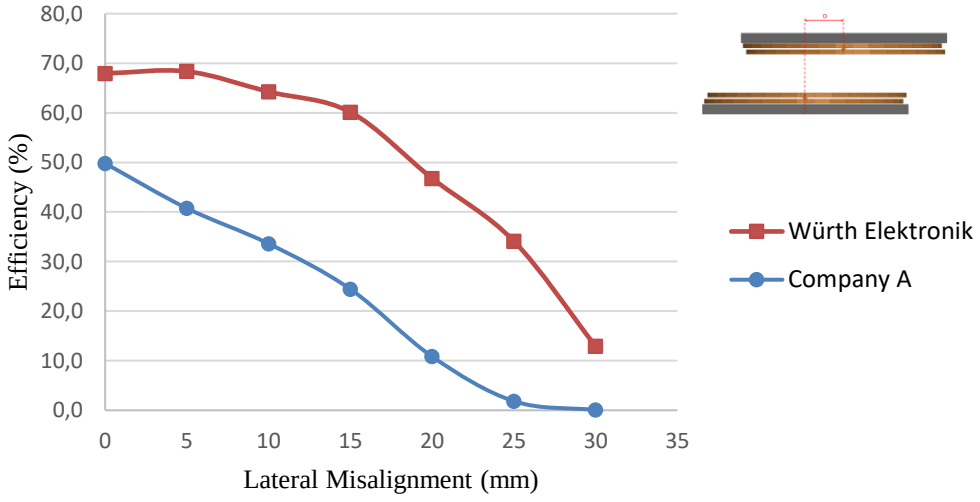

Figure 58 - Influence of the lateral misalignments in the efficiency of the WPT systems.

In Table 21, the obstacles tests using two massive obstacles of iron and aluminium with dimensions of 200*200*1.5 mm^3 are presented. These obstacles will be placed in the "middle" of both coils and above Rx coil. As expected by the results obtained in the previous chapter, with these obstacles in the middle of the path it is expected that there is no coupling between coils, so the efficiency should be zero or considerably close to it in both systems. However, both systems' efficiency differs a lot when placed above the receiver coil. In fact, since the Würth system is able to adapt its frequency to continue working in resonance, the system continues to be very efficient, in contrast with the "company A" system which in turn is adapted to the coils specific inductance and cannot handle any situation involving obstacles.

Table 21 - It is represented the influence of obstacles in the efficiency of the WPT systems.

	Company A	**Würth Elektronik**
Air	48,36%	80,99%
Middle iron	0%	0,96%
Above iron	0.01%	79,95%
Middle aluminium	0%	0%
Above aluminium	0%	77,66%

In general, the Würth system fits the initial requirements except for the temperature range. However, such temperature range requirement can be fulfilled with some component replacements. On the other hand, the "company A" system only accomplished the temperature range restriction. Nevertheless, they guarantee that in the future they could improve their system to fit the size requirements and improve efficiency. The overall results could be resumed in Table 22.

Table 22 - Overall WPT systems tests results.

	Range (mm)	**Max efficiency (%)**	**Delivered power (W)**
Company A	38	54	40
Würth Elektronik	220	81	47

4.2 Wireless communication

Regarding the purpose of this dissertation, it will be necessary to have a small module for wireless communication system capable of sending data accurately, securely, and with a minimum baud rate of 6.5 Mb/s. This system also needs to be joined with the WPT system, so a new antenna design will be presented. The tests will be made by measuring the baud rate of all the communication from the LiDAR's sensor to the vehicle's central intelligence in real time to process all the environmental information.

4.2.1 Communication modules

After analysing all the available options, the ESP32-WROOM-32U was the selected module. This module was selected because it is one of the smallest modules (18*19.2*0.8 mm^3) which supports both Ethernet and Wi-Fi with norms of ETH100 and 802.11 b/g/n. It also has a module with a U.FL connector to link an external antenna. This feature aided this module's importance when compared to the others, as it allowed the use of an antenna compatible with the WPT system and that is rotation invariant since it had always the same radiation pattern around the vertical axis rotation.

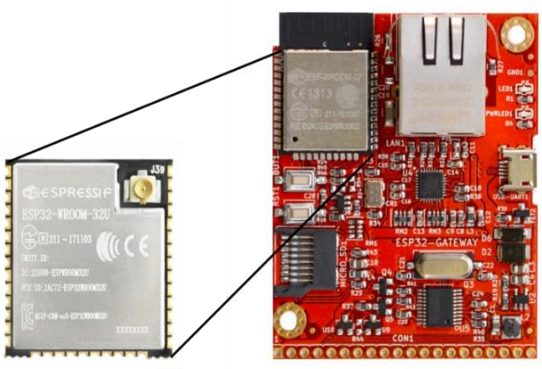

Figure 59 - ESP32-WROOM-32 replacement for the ESP32-WROOM-32U in the ESP32 GATEWAY devkit.

A development kit (devkit) was used to access the ESP32 interfaces. As aforementioned, this module was selected for having a high-speed data rate in physical and wireless connections. The usage of the Ethernet interface was imperative and one of the requirements to select the devkit was the RJ45 connector. After searching for several devkits with the ESP32 modules [56], not one with the module ESP32-WROOM-32U was found. Following on from Figure 59, the solution was to purchase a devkit with the ESP32-WROOM-32, which has the same pin layout and replace the modules. The selected development kit was the ESP32 GATEWAY and it was selected by convenience between the very few available. The result is presented in Figure 60.

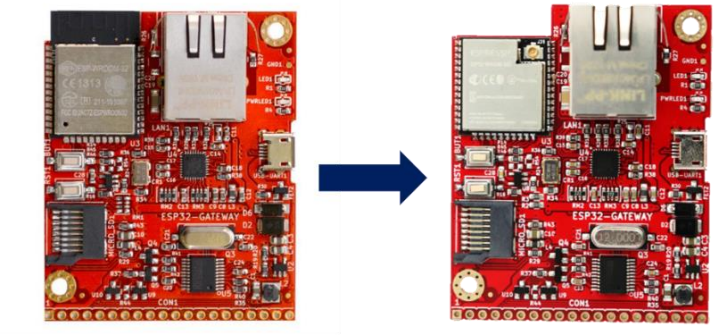

Figure 60 – Final result of the devkit.

Common wireless communication antennas are optimized to communicate at long distances. To send the information wirelessly, the data is sent by the transmitter antenna through electromagnetic (EM) fields. However, these fields are easily interrupted by a source with a powerful EM field. An EM amplifier at the same frequency as the communication that is close enough to the vehicle could blind the communication by radiating a powerful EM field however the information must not be interrupted because it will contain the LiDAR information. Therefore, using conventional antennas is not an option.

For a wireless communication in a vehicle environment, with low distance communication, where the security is the main concern, a new type of antenna could be utilized by implementing an antenna that communicates through magnetic fields. This field has a higher field attenuation with longer distances, which is normally a disadvantage, but in this specific case, it could be a good advantage, because it prevents much better any exterior perturbation.

The antenna will be formed by copper wire wrapped in the form of a flat coil, like Figure 61 suggests. The system will co-exist with a WPT system which uses identical coils to power the system. In order to take advantage of the environment, the antenna will share the already utilized elements to improve the efficiency of the WPT system (ferrite and possible shaft). These elements will also increase the security of the communication since the signal at the receiver is strong enough.

However, this antenna will not work like the conventional ones since this antenna will not radiate EM fields. The spiral format of the antenna will induce a magnetic field when a current flow through the antenna. This magnetic field will catch the receiver antenna which in turn will make the reverse process, inducting a current proportional to the one that flows in the transmitter whose signal encodes the information.

Due to the communication antenna's geometry (Figure 61), communication is immune to the rotation motion that the transmitter coil will be incorporated in the LiDAR's sensor.

Figure 61 - Communication antennas.

4.2.2 Communication link setup

To program the ESP32, a few steps were followed from [57]. The Arduino ide was set up to recognize some of the ESP32 boards and to compile the code before sending it to a board. Espressif provides an ESP 32 guide to aid the user in programming the ESP32-WROOM-32U. In the appendix the final code for the TX and RX boards is presented.

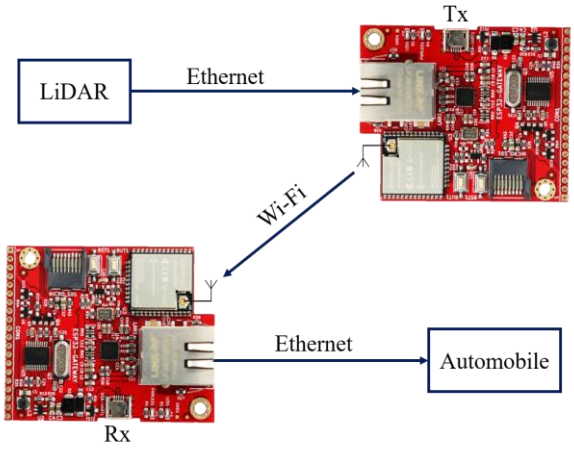

Figure 62 - Flux information illustration.

Considering the actual purpose of wireless communication, it was necessary to construct a network capable of including Wi-Fi and Ethernet connections with a secure communication protocol to prevent errors. The host (TX) receives data from the Ethernet interface and sends it via Wi-fi to the client (RX), which does the reverse process as suggested in Figure 62.

The first step was to create an access point in the host board, and program the client board to connect to it. The host only allows one client at a time to be connected because there is no need for more connections. Both behave as an Ethernet host when they create a connection with the LiDAR and the automobile in the case of the Tx and Rx respectively, by using a specific IP. After all the physical and wireless communications are made, a communication protocol is established.

The Transmission Control Protocol (TCP) abdicates from higher data transfers, to warrant that all the packets are delivered to the client without errors. Considering that the data to be transferred will contain the LiDAR information, there is no room for failure. To define how the modules manage their Wi-Fi and Ethernet communications, a thread for each connection was created. Using the Netconn API functions, a new TCP connection is established in each communication interface, and the data could flow without errors from the LiDAR to the automobile as illustrated in Figure 62.

4.2.3 Data rate performance assessment

After completing the module programming, the data rate of the communication between the LiDAR and the automobile was calculated. It was also important to assure that the information sent was correct with the help of a program which simulates the LiDAR and the automobile. This program is used in two different PCs. The first one sends several frames to the Tx module through an Ethernet interface, which sends them to the receiver via Wi-Fi. The information is ready to be sent by the Rx module to the second computer by an ethernet interface that will count the number of frames per second it receives as Figure 63 suggests.

Figure 63 - Lidar system program presenting the FPS between PC one and PC two.

In Figure 63, are presented the registered values, in frames per second (FPS), that are sent between the PCs. Each frame (red rectangle) is composed of a matrix of zeros and it has 450016 bits, which represents the LiDAR information. Each zero represents a red dot in the white rectangle. As Figure 63 suggests, all the information that reaches the second PC is red, so all the information was received correctly thanks to the TCP connection. By using this program, it is possible to find the actual communication rate as shown in Table 23. By connecting the Tx to the PC, through Ethernet and without any Wi-Fi connections, it is only possible to calculate the ethernet baud rate. In this way it is possible to collect the actual Ethernet velocity presented in Table 23. The same mechanism can possibly measure the Wi-Fi data rate.

Table 23 - Lidar system results for each test

	Only ETH	**Only Wi-Fi**	**ETH + Wi-Fi**
FPS	60	19	15
Baud rate (Mbits/s)	27	8,55	6,75

Regarding the communication data rate requirements, the obtained 6.75 Mbits/s (15 FPS) are slightly above the limit to meet the required 6.5 Mbit/s. However, the obtained results varied around 15 FPS, so Table 23 presents the mean values. To achieve a stable and if possible higher FPS, it is necessary to improve the communication.

4.3 Co-design setup

In this section a co-design between both wireless systems will be presented. The Würth system will be utilized for the wireless power system. Both systems' antennas are coils that will induct magnetic fields. Each field will have a very different frequency since the WPT system works around 100 kHz and the wireless communication works at 2,4 GHz.

Figure 64 - Coils Co-design.

The co-design of both wireless systems coils is illustrated in Figure 64, with the communication coil being located inside the WPT coil. This design was planned so the WPT coils operates as a shield of the wireless communication. After testing both systems

simultaneously, it was observed that both work without interference, thanks to their frequency difference.

A co-design setup (Figure 65) was designed by LiDAR's mechanic team in order to test how both systems work under the final LiDAR system conditions. The WPT receiver and the wireless communication transmitter will be in the rotor part of the whole system, while the WPT transmitter module and the wireless communication receiver module will be in a stationary part physically connected to the vehicle.

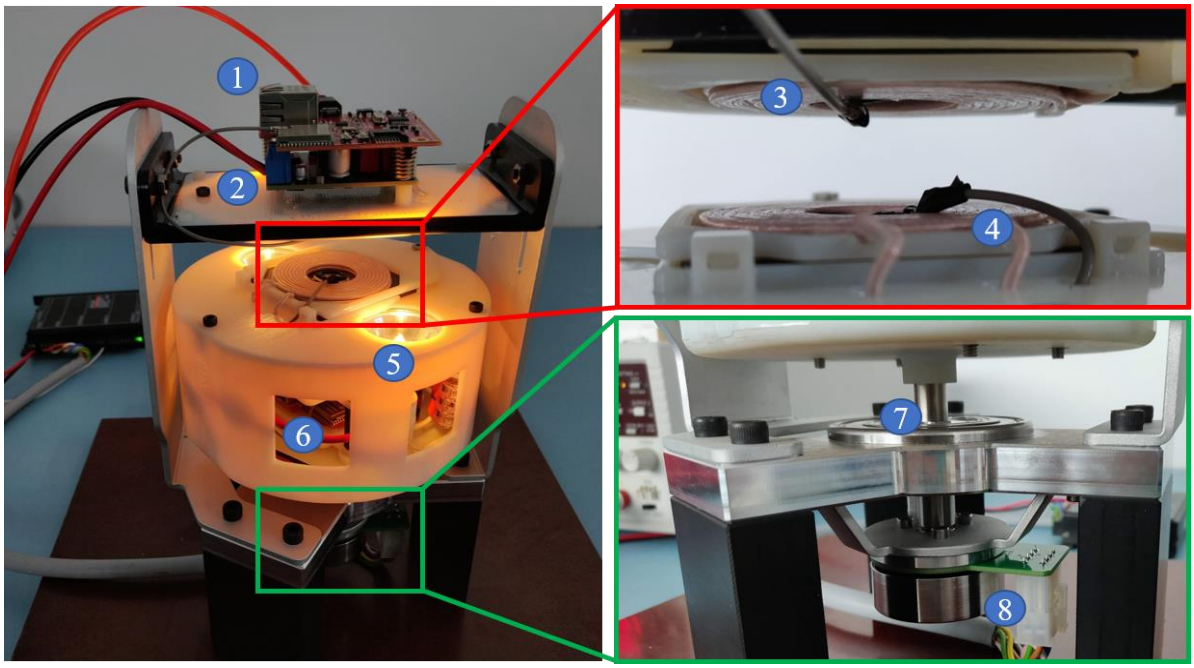

Figure 65 - The co-design setup. 1 represents the Rx communication module; 2 represents the WPT Tx module; 3 and 4 represents the coils co-design of both wireless systems;5 represents the load of the system (2 lamps); 6 represents the rotate part with the Rx WPT and Tx communication modules; 7 represents the rotor shaft; 8 the motor that makes the 6 rotate.

When the motor is turned off, the obtained stationary results confirm those presented in section 4.1.2. After turning on the motor, the consumed current decreases about 20 mA. This small change could be explained by the minimal misalignment existing in the motor, in which the rotor part will oscillate generating small angular and lateral misalignments, since it is expected that for a perfect alignment, the rotation would not influence the transference of energy. However, this slight power consumption reduction does not significantly change the resulting efficiency.

CHAPTER 5 CONCLUSIONS

Wireless power and data transfer systems are part of the technologies that have been ascending throughout the last years, with wireless communication already playing a very important role in modern society. Considering the two techniques of wireless power transfer in the near-field region, the use of the inductive coupling technique was chosen due to its advantages comparatively to capacitive coupling.

The inductive coupling is normally more efficient when dealing with distances between plates greater than 1mm [58] and less dangerous when it is required to transfer high power, due to the high voltages stored in the capacitive plates [25]. Considering that a power transfer around 10 mm OTA was requested, efficiency was one of the principal requirements for the system and therefore, it was decided to use the inductive coupling method in the final WPT system. When considering the co-design, the possibility of accomplishing this with two different antennas (one for each wireless system) remains.

The wireless communication system was chosen considering its size and its baud rate both in wireless and physical interfaces. The LiDAR sensor uses Ethernet to communicate with the module. This module needs to recognize the Ethernet communication and send the received information wirelessly to the receiver module which will do exactly the opposite. Regarding the available options, a small module (ESP32-WROOM-32) with ETH 100 and 802.11 b/g/n was considered a viable solution. This module also features an U.FL connector for an external antenna which will facilitate the co-design.

Coils were simulated for the wireless power system using the HFSS software. A coils' parametric study was conducted to better understand how each factor influences the coil's inductance and its coupling coefficient with the other coil. In the coils' parameters, the influence of the number of turns, separation between turns, number of layers and the inner radius were tested. The distance between coils, lateral and angular misalignments were also part of the study. The influence of exterior factors such as different ferrite designs, obstacles near the coils, and a possible shaft that goes through the middle of both coils were tested as well. These tests were made to evaluate possible setups when the WPT system is incorporated in the LiDAR system.

In general, considering that the size of the coils remains the same while the self-inductance of the coil increases with the increasing of the number of turns and the decreasing of the inner radius. Hence, it is important to adapt the inner radius to the smaller value possible depending on the system's final design. The distance between coils has a significant impact on the coils coupling. Fortunately, lateral and angular misalignments have smoother impacts. Therefore, for a well-fixed system, small misalignments of millimetres will not influence the coupling between the coils. However, it is important to have the coils as close as possible to guarantee good coupling. The ferrite, which will enhance the magnetic flux, will have a flat block behind the coil with a small nucleus in the middle of the wires. This material behind the coil represents a major breakthrough, as it helps to increase the coupling coefficient alongside with the self-inductance. In order to implement a shaft in the system, several materials were tested with iron being the one that produced the best results. Nevertheless, this material needs to be laminated due to the strong eddy currents induced inside of it. Obstacles near the WPT coils can also be problematic due to eddy currents, leading to the necessity of preparing the best design possible near the WPT system.

The selected wireless power system was a module of the company Würth Elektronik. "Company A" also sent a prototype for testing purposes only. The first system comes with a series of advantages like its size, power deliver and the possibility of changing components, contrary to the second system which did not fit the size requirements, and comes sealed by the company for protective reasons. After the misalignment, the distance between coils and the obstacles tests, the Würth system presented the best results with the highest efficiency (81%). This system also works better with short distances seeing that the efficiency is fixed in the first 15 mm between coils. In addition, it has much better results near obstacles, considering that the efficiency remains around the same values when the obstacle is above the Rx coil. The "company A" system cannot transfer any energy in that situation.

The chosen power transfer system (Würth Elektronik boards) meets most of the requirements presented in the first chapter. Only the temperature requirement is an issue. However, thanks to its project files, it is possible to change some components of the board to fit all the requirements. The maximum obtained efficiency value is 81% and it is kept around this value for distances between coils of up to 15 mm. This system presents very good results for the presence of obstacles out of the path. When an iron and an aluminium plate is placed

above the Rx coil, the whole system's efficiency drops to 79,95% and 77,66%, respectively. The maximum power delivery of the system is 47 W and the range is of 220 mm.

The wireless communication system was the ESP32-WROOM-32U module built in the ESP32 GATEWAY devkit. This module has the particular feature of having an U.FL connector to link an external antenna. Two codes presented in the appendix were developed for both the transmitter and the receiver module. The transmitter module was programmed with the aim of receiving data from LiDAR through an Ethernet interface, and then sending it to the receiver module via Wi-Fi. The receiver is programmed to receive that data via Wi-Fi and to send it to the automobile's central intelligence via an Ethernet interface.

The communication antennas were designed as coils to guarantee a good co-design with the WPT system and to improve their resistance to external intrusions. A program that simulates the work of LiDAR and the automobile sends or receives several matrixes with information by Ethernet. With this simulation, a baud rate of 6,75 Mbit/s from LiDAR to the vehicle is obtained.

A co-design setup was built to test both systems together. The tested co-design between the two chosen systems proves the possibility of linking those two systems without any interference between them. The obtained results were met as expected, since the rotative results were mostly the same as the stationary ones.

5.1 Future work

Although the co-design was successfully made, some changes and improvements need to be made to both wireless systems.

In the wireless power transfer system, it is necessary to change some components to meet the temperature requirements. The WPT coil was not manufactured considering the results in chapter 3. Thus, after defining all the LiDAR's design, it is necessary to design a coil according to the available space, in order to maximize the coupling between transmitter and the receiver.

As a topic of extreme importance, the EMC will be the next big step after this dissertation. The EMC limits are non-trivial, especially in this type of coupling. However, by using an appropriate housing, it is possible to manage this issue. As this system will be part of

a rotative LiDAR's sensor, which includes a lot of other systems, this housing will be designed alongside the design team of the LiDAR. In order for the limits to be respected, the improvement of the WPT and wireless communication co-design is of major importance for a reduction to the EMC's impact in the final system.

In the wireless communication system, the LiDAR sensor is in a progressive stage, and faster data transfer is constantly needed. Consequently, a new type of wireless communication is required, because the developed one is at the limit of the required baud rate. To prevent external clients from connecting to the transmitter, every time the transmitter access point receives a client, the idea is to verify the identity of the client with a key recognised by the two modules. If the wrong device is connected to the host, it closes the connection and waits until a new one tries to connect, repeating the process until a certified client is found.

A new PCB design for the communication antenna is also a target for future work since the actual communication coils are fragile. By printing a coil and connecting it to a potentiometer, it is possible to adapt the impedance of the PCB antenna. Therefore, with this method, the antennas may be accustomed to the final LiDAR system design.

REFERENCES

[1] T. J. Gretk and A. Kurs, “Power Transfer Through Strongly Coupled Resonances by Andr6 Kurs Submitted to the Department of Physics in partial fulfillment of the requirements for the degree of at the Thesis Supervisor Accepted by Power Transfer Through Strongly Coupled Resonances by,” 2007.

[2] A. Abdolkhani, *Wireless Power Transfer - Fundamentals and Technologies*, vol. 3. 2016.

[3] J. I. Agbinya, *Wireless power transfer*. River Publishers, 2012.

[4] Marie Christiano, “Introduction to Wireless Power Transfer.” [Online]. Available: https://www.allaboutcircuits.com/technical-articles/introduction-to-wireless-power-transfer-wpt/. [Accessed: 18-Jan-2018].

[5] “File:FarNearFields-USP-4998112.svg - Wikimedia Commons.” [Online]. Available: https://commons.wikimedia.org/wiki/File:FarNearFields-USP-4998112.svg. [Accessed: 18-Jan-2018].

[6] C. Coleman, *An Introduction to Radio Frequency Engineering*. Cambridge University Press, 2004.

[7] A. Karalis, J. D. Joannopoulos, and M. Soljačić, “Efficient wireless non-radiative mid-range energy transfer,” *Ann. Phys. (N. Y).*, vol. 323, no. 1, pp. 34–48, Jan. 2008.

[8] A. Gopinath, “All About Transferring Power Wirelessly,” *Electron. You E-zine*, pp. 52–56, 2013.

[9] B. M. Huschens and M. E. Europe, “Various techniques for wireless charging,” pp. 1–4, 2012.

[10] S. Valtchev, E. Baikova, and L. Jorge, “Electromagnetic field as the wireless transporter of energy,” *Facta Univ. - Ser. Electron. Energ.*, vol. 25, no. 3, pp. 171–181, 2012.

[11] “Wireless Power Transfer.” [Online]. Available: https://en.wikipedia.org/wiki/Wireless_power_trans. [Accessed: 19-Jan-2018].

[12] M. S. Bakir and J. D. Meindl, *Integrated interconnect technologies for 3D nanoelectronic systems*. Artech House, 2009.

[13] A. Kurs, A. Karalis, R. Moffatt, J. D. Joannopoulos, P. Fisher, and M. Soljacic, “Wireless power transfer via strongly coupled magnetic resonances.,” *Science*, vol. 317, no. 5834, pp. 83–86, 2007.

[14] S. Valtchev, E. Baikova, and L. Jorge, “Electromagnetic field as the wireless transporter of energy,” *Facta Univ. - Ser. Electron. Energ.*, vol. 25, no. 3, pp. 171–181, 2012.

[15] C. T. C. O. S. and H. Administration, *Electromagnetic Radiation and How It Affects Your Instruments. Near field vs. Far field.* U.S. Dept of Labor, 1990.

[16] G. A. Landis, “Re-evaluatigng Satellite Solar Power Systems for Earth,” *IEEE 4th World Conf. Photovolt. Energy Convers.*, pp. 1939–1942, 2006.

[17] L. J. Rodríguez-aragón, “Informática Básica Internet y Teleinformática,” 2008.

[18] “Wireless communication basics.” [Online]. Available: https://www.lynda.com/Software-Development-tutorials/Wireless-communication-basics/533280/608397-4.html. [Accessed: 29-Jan-2018].

[19] N. O. and A. A. US Department of Commerce, “What is LIDAR.” [Accessed: 03-Mar-2018]

[20] A. M. Sodagar and P. Amiri, “Capacitive coupling for power and data telemetry to implantable biomedical microsystems,” *2009 4th Int. IEEE/EMBS Conf. Neural Eng. NER ’09*, pp. 411–414, 2009.

[21] S. Goma, “Murata Taps Capacitive-Coupled Method for wireless power transfer,” *AEI Novemb.*, 2011.

[22] F. Lu, H. Zhang, and C. Mi, “A Two-Plate Capacitive Wireless Power Transfer System for Electric Vehicle Charging Applications,” *IEEE Trans. Power Electron.*, vol. 33, no. 2, pp. 964–969, 2018.

[23] C. K. Chang, G. G. Da Silva, A. Kumar, S. Pervaiz, and K. K. Afridi, “30 W capacitive wireless power transfer system with 5.8 pF coupling capacitance,” *2015 IEEE Wirel. Power Transf. Conf. WPTC 2015*, pp. 30–33, 2015.

[24] muRata innovator in electronics, “Capacitive Coupling Wireless Power Transmission System | Murata Manufacturing Co., Ltd.” [Online]. Available: http://www.murata.com/about/newsroom/techmag/metamorphosis16/productsmarket/wireless. [Accessed: 26-Sep-2017].

[25] D. Rozario, “Design of Contactless Capacitive Power Transfer Systems for Battery Charging Applications,” pp. 1–115, 2016.

[26] U. C. Berkeley, “Roadway Powered Electric Vehicle Project Parametric Studies: Phase 3D Final Report,” *Calif. Partn. Adv. transit Highw.*, 1996.

[27] W.-T. Chen, R. A. Chinga, S. Yoshida, J. Lin, and C. Hsu, “A 36W Wireless Power

Transfer System with 82% Efficiency for LED Lighting Applications," *Transcations Japan Inst. Electron. Packag.*, vol. 6, no. 1, pp. 32–37, 2013.

[28] S. M. Kim, J. I. Moon, S. W. Kim, and I. K. Cho, "120 W wireless power transfer system for the wireless seat in automobile," *Prog. Electromagn. Res. Symp.*, vol. 2018–Novem, pp. 2635–2637, 2018.

[29] T. Imura, H. Okabe, and Y. Hori, "Basic experimental study on helical antennas of wireless power transfer for electric vehicles by using magnetic resonant couplings," *5th IEEE Veh. Power Propuls. Conf. VPPC '09*, pp. 936–940, 2009.

[30] "POWER REPUBLIC." [Online]. Available: http://en.power-republic.com/. [Accessed: 02-Feb-2018].

[31] T. Proxi-module, "Proxi-Module 100W - PowerbyProxi," no. February, pp. 1–14, 2017.

[32] "Apple acquires wireless charging company PowerbyProxi." [Online]. Available: https://www.engadget.com/2017/10/25/apple-wireless-charging-powerbyproxi/. [Accessed: 02-Feb-2018].

[33] "Ferro Solutions." [Online]. Available: http://www.ferrosi.com/. [Accessed: 28-Nov-2017].

[34] "WE Home | Würth Elektronik (Wurth Electronics) Group." [Online]. Available: https://www.we-online.com/web/en/wuerth_elektronik/start.php. [Accessed: 15-Nov-2017].

[35] H. Power and W. Power, "High Power Wireless Power Transfer," pp. 1–26, 2016.

[36] Y. Zhang, H. Tang, C. Yao, Y. Li, and S. Xiao, "Experiments on adjustable magnetic metamaterials applied in megahertz wireless power transmission," *AIP Adv.*, vol. 5, no. 1, 2015.

[37] J. Wang, B.; Teo, K.H.; Nishino, T.; Yerazunis, W.; Barnwell, J.; Zhang, "Wireless power transfer with metamaterials," *Antennas Propag. (EUCAP), Proc. 5th Eur. Conf.*, pp. 3905–3908, 2011.

[38] M. Chabalko, J. Besnoff, and D. Ricketts, "Magnetic field enhancement in wireless power using metamaterials magnetic resonant couplers.," *IEEE Antennas Wirel. Propag. Lett.*, vol. 1, no. c, pp. 1–1, 2015.

[39] T. Versloot, D. Barker, and X. One, "Optimization of Near-Field Wireless Power Transfer Using Evolutionary Strategies," *Esa.Int*, pp. 2436–2440.

[40] J. Seth, "Ferrite loaded coils for improved wireless power transfer efficiency NAVAL

POSTGRADUATE," 2015.

[41] N. Oodachi, K. Ogawa, H. Kudo, H. Shoki, S. Obayashi, and T. Morooka, "Efficiency improvement of wireless power transfer via magnetic resonance using transmission coil array," *IEEE Antennas Propag. Soc. AP-S Int. Symp.*, pp. 1707–1710, 2011.

[42] L. Rakotondrainibe, Y. Kokar, G. Zaharia, and G. El Zein, "60 GHz High Data Rate Wireless Communication System," *VTC Spring 2009 - IEEE 69th Veh. Technol. Conf.*, pp. 1–5, 2009.

[43] T. Baykas *et al.*, "IEEE 802.15.3c: The first IEEE wireless standard for data rates over 1 Gb/s," *IEEE Commun. Mag.*, vol. 49, no. 7, pp. 114–121, 2011.

[44] X. Wang, Y. Ren, J. Zhao, Z. Guo, and R. Yao, "Comparison of IEEE 802.11e and IEEE 802.15.3 MAC," in *Proceedings of the IEEE 6th Circuits and Systems Symposium on Emerging Technologies: Frontiers of Mobile and Wireless Communication (IEEE Cat. No.04EX710)*, 2004, vol. 2, p. 675–680 Vol.2.

[45] "Bluetooth V4.0 HM-11 BLE Module." [Online]. Available: http://wiki.seeedstudio.com/Bluetooth_V4.0_HM_11_BLE_Module/. [Accessed: 22-Jan-2018].

[46] "Wireless Ethernet: 802.11n And Bluetooth - LAN 101: Networking Basics." [Online]. Available: https://www.tomshardware.com/reviews/local-area-network-wi-fi-wireless,3020-6.html. [Accessed: 22-Jan-2018].

[47] T. Brief, "GainSpan GS1500M." Shared by GainSpan.

[48] L. Ji, L. Wang, C. Liao, and S. Li, "Simultaneous Wireless Power and Bidirectional Information Transmission with a Single-Coil, Dual-Resonant Structure," *IEEE Trans. Ind. Electron.*, vol. 46, no. c, 2018.

[49] C. Huang, H. Jian, J. Kao, C. Lin, and Y. Kuo, "New Design of Wireless Power and Bidirectional Data Transmission," *2017 12th IEEE Conf. Ind. Electron. Appl.*, pp. 374–379, 2017.

[50] L. M. Camarinha-Matos, A. J. Falcão, N. Vafaei, and S. Najdi, "Technological innovation for cyber-physical systems: 7th IFIP WG 5.5/SOCOLNET advanced doctoral conference on computing, electrical and industrial systems, DoCEIS 2016 Costa de Caparica, Portugal, April 11–13, 2016 proceedings," *IFIP Adv. Inf. Commun. Technol.*, vol. 470, pp. 293–301, 2016.

[51] G. Yilmaz and C. Dehollain, *Wireless Power Transfer and Data Communication for*

Neural Implants. 2017.

[52] “Wireless Power & Communication - WPC -.” [Online]. Available: http://www.wpc.no/. [Accessed: 21-Nov-2017].

[53] S. Davis, “Wireless power minimizes interconnection problems,” *Power Electron. Technol.*, pp. 10–14, 2011.

[54] “Eddy current.” [Online]. Available: https://en.wikipedia.org/wiki/Eddy_current. [Accessed: 02-Jun-2018].

[55] “WPC 50W12- 24V-3A_sch.pdf.” Shared by Wurth Elektroniks.

[56] “ESP32.” [Online]. Available: http://esp32.net/. [Accessed: 13-Jan-2018].

[57] “ESP-IDF Programming Guide — ESP-IDF Programming Guide v3.2-dev-141-ga3c4325 documentation.” [Online]. Available: https://esp-idf.readthedocs.io/en/latest/index.html. [Accessed: 05-Feb-2018].

[58] J. Dai and D. C. Ludois, “A Survey of Wireless Power Transfer and a Critical Comparison of Inductive and Capacitive Coupling for Small Gap Applications,” *IEEE Trans. Power Electron.*, vol. 30, no. 11, pp. 6017–6029, 2015.

APPENDIX I – COMMUNICATION HOST CODE

```
#include <WiFi.h>
#include <ETH.h>
#include <stdio.h>
#include <string.h>

#include "esp_system.h"
#include "esp_err.h"
#include "esp_event_loop.h"
#include "esp_event.h"
#include "esp_attr.h"
#include "esp_log.h"
#include "esp_eth.h"
#include "lwip/sys.h"
#include "lwip/api.h"
#include "stdbool.h"
#include "lwip/ip_addr.h"

#include <arpa/inet.h>

#include "eth_phy/phy_lan8720.h"
#define DEFAULT_ETHERNET_PHY_CONFIG phy_lan8720_default_ethernet_config

#define ETH_CLK_MODE    ETH_CLOCK_GPIO17_OUT

//-1 to disable the signal for external crystal
#define ETH_POWER_PIN   -1

// Ethernet PHY type(LAN8720)
#define ETH_TYPE        ETH_PHY_LAN8720

// address of Ethernet PHY (0 or 1 for LAN8720)
#define ETH_ADDR       0

// clock signal for the Ethernet PHY
#define ETH_MDC_PIN     23

// IO signal for the Ethernet PHY
#define ETH_MDIO_PIN    18

static bool eth_connected = false;

static void eth_gpio_config_rmii(void)
{
    // TXD0 = GPIO19
```

```
45      // TXD1 = GPIO22
46      // TX_EN = GPIO21
47      // RXD0 = GPIO25
48      // RXD1 = GPIO26
49      // CLK == GPIO0
50      phy_rmii_configure_data_interface_pins();
51      phy_rmii_smi_configure_pins(ETH_MDC_PIN, ETH_MDIO_PIN);
52  }
53
54  #define IP_DEFAULT_ADDRESS_ETH              "192.168.0.10"
55  #define IP_DEFAULT_NETMASK_ETH              "255.255.255.0"
56  #define IP_DEFAULT_GATEWAY_ETH              "192.168.0.1"
57
58  IPAddress IP_DEFAULT_ADDRESS_WIFI(192,168,10,10);
59  IPAddress IP_DEFAULT_NETMASK_WIFI(255,255,255,0);
60  IPAddress IP_DEFAULT_GATEWAY_WIFI(192,168,10,9);
61
62  const char* ssid     = "ESP32";
63  const char* passphrase = "password";
64  int max_connections = 1;
65
66  struct netconn *conn_eth, *conn_wifi;
67  bool b_eth=0, b_wifi=0;
68
69  void tcpclient_eth(void *arg)
70  {
71    struct netbuf *buf;
72    void *data;
73    u16_t len;
74
75            Serial.println("Ethernet Client Connected");
76            b_eth=1;
77
78            while (netconn_recv(conn_eth, &buf) == ERR_OK)
79            {
80              do
81              {
82                netbuf_data(buf, &data, &len);
83                if (b_wifi ==1) netconn_write(conn_wifi, data, len,
NETCONN_COPY);
84
85              }
86              while (netbuf_next(buf) >= 0);
87
88              netbuf_delete(buf);
89            }
```

```
 90
 91            netconn_close(conn_eth);
 92            netconn_delete(conn_eth);
 93            Serial.println("Ethernet Client Disconnected");
 94
 95            b_eth=0;
 96
 97            vTaskDelete(NULL);
 98 }
 99
100 void tcpclient_wifi(void *arg)
101 {
102   struct netbuf *buf;
103   void *data;
104   u16_t len;
105
106            Serial.println("WiFi Client Connected");
107            b_wifi=1;
108
109            while (netconn_recv(conn_wifi, &buf) == ERR_OK)
110            {
111              do
112              {
113                netbuf_data(buf, &data, &len);
114                if (b_eth ==1) netconn_write(conn_eth, data, len,
NETCONN_COPY);
115
116              }
117              while (netbuf_next(buf) >= 0);
118
119              netbuf_delete(buf);
120            }
121
122            netconn_close(conn_wifi);
123            netconn_delete(conn_wifi);
124            Serial.println("WiFi Client Disconnected");
125
126            b_wifi=0;
127
128            vTaskDelete(NULL);
129 }
130
131
132 void tcpecho_thread(void* arg)
133 {
134   err_t err, accept_err;
```

```
135   struct netconn *conn, *newconn;
136
137   LWIP_UNUSED_ARG(arg);
138
139   // Create a new connection
140   conn = netconn_new(NETCONN_TCP);
141
142   if (conn!=NULL)
143   {
144     // Bind connection to the port 5000
145     err = netconn_bind(conn, NULL, 5000);
146
147     if (err == ERR_OK)
148     {
149       //connection stays in listen mode
150       netconn_listen(conn);
151       while (1)
152       {
153         // Grab new connection
154          accept_err = netconn_accept(conn, &newconn);
155         // Process the new connection
156         if (accept_err == ERR_OK)
157         {
158           //identify the type of connection (Ethernet or WiFi)
159           ip_addr_t addr;
160           u16_t port;
161           netconn_getaddr(newconn, &addr, &port, 1);
162           char *addr_m=inet_ntoa(addr);
163           if(strstr(addr_m, "192.168.0") != NULL && b_eth==0) {
164             conn_eth=newconn;
165             Serial.printf("Ethernet IP address=%s\n", addr_m);
166             xTaskCreate( tcpclient_eth, "tcp_client_Eth",
configMINIMAL_STACK_SIZE * 5, NULL, 1, NULL );
167           }
168           else if(strstr(addr_m, "192.168.10") !=NULL && b_wifi==0){
169             conn_wifi=newconn;
170             Serial.printf("WiFi IP address=%s\n", addr_m);
171             xTaskCreate( tcpclient_wifi, "tcp_client_WiFi",
configMINIMAL_STACK_SIZE * 5, NULL, 1, NULL );
172           }
173           else{
174             netconn_close(newconn);
175             netconn_delete(newconn);
176           }
177         }
178       }
```

```
179     }
180     else
181     {
182       netconn_delete(newconn);
183     }
184   }
185   vTaskDelete(NULL);
186 }
187
188 void tcpecho_init(void)
189 {
190   xTaskCreate( tcpecho_thread, "tcpecho_thread",
configMINIMAL_STACK_SIZE * 5, NULL, 1, NULL );
191 }
192
193 void setup() {
194
195     bool ret;
196
197     Serial.begin(115200);
198
199     // We start by connecting to a WiFi network
200
201     Serial.println();
202     Serial.println();
203     Serial.print("Take Online ... ");
204     Serial.println(ssid);
205
206     WiFi.softAPConfig(IP_DEFAULT_ADDRESS_WIFI, IP_DEFAULT_GATEWAY_WIFI,
IP_DEFAULT_NETMASK_WIFI);
207     ret = WiFi.softAP(ssid, passphrase, 1, 0, max_connections);
208     WiFi.softAPConfig(IP_DEFAULT_ADDRESS_WIFI, IP_DEFAULT_GATEWAY_WIFI,
IP_DEFAULT_NETMASK_WIFI);
209
210     Serial.println("");
211     Serial.println("WiFi AP online ...");
212     Serial.println(WiFi.softAPIP());
213
214     tcpip_adapter_init();
215     tcpip_adapter_dhcpc_stop(TCPIP_ADAPTER_IF_ETH); // Don't run a DHCP
client
216     tcpip_adapter_ip_info_t ipInfo;
217     ip4addr_aton(IP_DEFAULT_ADDRESS_ETH, &ipInfo.ip);
218     ip4addr_aton(IP_DEFAULT_GATEWAY_ETH, &ipInfo.gw);
219     ip4addr_aton(IP_DEFAULT_NETMASK_ETH, &ipInfo.netmask);
```

```
220     ESP_ERROR_CHECK(tcpip_adapter_set_ip_info(TCPIP_ADAPTER_IF_ETH,
&ipInfo));
221
222     eth_config_t phyConfig = DEFAULT_ETHERNET_PHY_CONFIG;
223     phyConfig.phy_addr = PHY0;
224     phyConfig.gpio_config = eth_gpio_config_rmii;
225     phyConfig.tcpip_input = tcpip_adapter_eth_input;
226     ESP_ERROR_CHECK(esp_eth_init(&phyConfig));
227     ESP_ERROR_CHECK(esp_eth_enable());
228
229     ESP_ERROR_CHECK(tcpip_adapter_get_ip_info(TCPIP_ADAPTER_IF_ETH,
&ipInfo));
230     printf("main: Network started on "IPSTR"\n", IP2STR(&ipInfo.ip));
231
232     tcpecho_init();
233
234 }
235 void loop(){
236
237 }
```

APPENDIX II – COMMUNICATION CLIENT CODE

```
#include <WiFi.h>
#include <ETH.h>
#include <stdio.h>
#include <string.h>

#include "esp_system.h"
#include "esp_err.h"
#include "esp_event_loop.h"
#include "esp_event.h"
#include "esp_attr.h"
#include "esp_log.h"
#include "esp_eth.h"
#include "lwip/sys.h"
#include "lwip/api.h"
#include "stdbool.h"
#include "lwip/ip_addr.h"
#include "lwip/ip4_addr.h"

#include <arpa/inet.h>

#include <driver/adc.h>

#include "eth_phy/phy_lan8720.h"
#define DEFAULT_ETHERNET_PHY_CONFIG phy_lan8720_default_ethernet_config

#define ETH_CLK_MODE    ETH_CLOCK_GPIO17_OUT

//-1 to disable the signal for external crystal
#define ETH_POWER_PIN   -1

// Ethernet PHY type(LAN8720)
#define ETH_TYPE        ETH_PHY_LAN8720

// address of Ethernet PHY (0 or 1 for LAN8720)
#define ETH_ADDR       0

// clock signal for the Ethernet PHY
#define ETH_MDC_PIN     23

// IO signal for the Ethernet PHY
#define ETH_MDIO_PIN    18


static bool eth_connected = false;
```

```
45
46 static void eth_gpio_config_rmii(void)
47 {
48     // RMII data pins are fixed:
49     // TXD0 = GPIO19
50     // TXD1 = GPIO22
51     // TX_EN = GPIO21
52     // RXD0 = GPIO25
53     // RXD1 = GPIO26
54     // CLK == GPIO0
55     phy_rmii_configure_data_interface_pins();
56     phy_rmii_smi_configure_pins(ETH_MDC_PIN, ETH_MDIO_PIN);
57 }
58
59 #define IP_DEFAULT_ADDRESS_ETH              "192.168.0.10"
60 #define IP_DEFAULT_NETMASK_ETH              "255.255.255.0"
61 #define IP_DEFAULT_GATEWAY_ETH              "192.168.0.1"
62
63 IPAddress IP_DEFAULT_ADDRESS_WIFI(192,168,10,10);
64 IPAddress IP_DEFAULT_NETMASK_WIFI(255,255,255,0);
65 IPAddress IP_DEFAULT_GATEWAY_WIFI(192,168,10,9);
66
67 #define remote_ip ((u32_t)0xC0A80A0AUL)
68
69 const char* ssid     = "ESP32";
70 const char* passphrase = "password";
71
72 // digital pin 2 has a pushbutton attached to it. Give it a name:
73 int pushButton = 34;
74 bool send_state = 0;
75
76 struct netconn *conn_eth, *conn_wifi, *conn, *conn_client;
77 bool b_eth=0, b_wifi=0;
78
79 void tcpclient_eth(void *arg)
80 {
81   struct netbuf *buf;
82   void *data;
83   u16_t len;
84
85           Serial.println("Ethernet Client Connected");
86           b_eth=1;
87
88           while (netconn_recv(conn_eth, &buf) == ERR_OK)
89           {
90             do
```

```
 91              {
 92                netbuf_data(buf, &data, &len);
 93                if (b_wifi ==1) netconn_write(conn_wifi, data, len,
NETCONN_COPY);
 94
 95              }
 96              while (netbuf_next(buf) >= 0);
 97
 98              netbuf_delete(buf);
 99            }
100
101            netconn_close(conn_eth);
102            netconn_delete(conn_eth);
103            Serial.println("Ethernet Client Disconnected");
104
105            b_eth=0;
106
107            vTaskDelete(NULL);
108 }
109
110 void tcpclient_wifi(void *arg)
111 {
112   struct netbuf *buf;
113   void *data;
114   u16_t len;
115
116            Serial.println("WiFi Client Connected");
117            b_wifi=1;
118
119            while (netconn_recv(conn_wifi, &buf) == ERR_OK)
120            {
121              do
122              {
123                netbuf_data(buf, &data, &len);
124                if (b_eth ==1) netconn_write(conn_eth, data, len,
NETCONN_COPY);
125              }
126              while (netbuf_next(buf) >= 0);
127
128              netbuf_delete(buf);
129            }
130
131            netconn_close(conn_wifi);
132            netconn_delete(conn_wifi);
133            Serial.println("WiFi Client Disconnected");
134
```

```
135           b_wifi=0;
136
137           vTaskDelete(NULL);
138 }
139
140
141 void tcpecho_thread(void* arg)
142 {
143   err_t err, accept_err;
144   struct netconn *newconn;
145
146   LWIP_UNUSED_ARG(arg);
147
148   // Create a new connection
149   conn = netconn_new(NETCONN_TCP);
150
151   if (conn!=NULL)
152   {
153     // Bind connection to the port 5000
154     err = netconn_bind(conn, NULL, 5000);
155
156     if (err == ERR_OK)
157     {
158       //connection stays in listen mode
159       netconn_listen(conn);
160       while (1)
161       {
162         // Grab new connection
163          accept_err = netconn_accept(conn, &newconn);
164         // Process the new connection
165         if (accept_err == ERR_OK)
166         {
167           //identify the type of connection (Ethernet or WiFi)
168           ip_addr_t addr;
169           u16_t port;
170           netconn_getaddr(newconn, &addr, &port, 1);
171           char *addr_m=inet_ntoa(addr);
172           if(strstr(addr_m, "192.168.0") != NULL && b_eth==0) {
173             conn_eth=newconn;
174             Serial.printf("Ethernet IP address=%s\n", addr_m);
175             xTaskCreate( tcpclient_eth, "tcp_client_Eth",
configMINIMAL_STACK_SIZE * 5, NULL, 1, NULL );
176           }
177           else{
178             netconn_close(newconn);
179             netconn_delete(newconn);
```

```
180           }
181
182
183         }
184
185       }
186     }
187     else
188     {
189       netconn_delete(newconn);
190     }
191   }
192   vTaskDelete(NULL);
193 }
194
195 void tcpecho_init(void)
196 {
197   xTaskCreate( tcpecho_thread, "tcpecho_thread",
configMINIMAL_STACK_SIZE * 5, NULL, 1, NULL );
198 }
199
200 void wifi_connection (){
201 //connect to the Host acess point
202 err_t err, err2;
203 ip_addr_t ipremote;
204 u16_t port;
205 conn_client = netconn_new(NETCONN_TCP);
206
207         if (conn_client!=NULL)
208         {
209             IP_ADDR4 (&ipremote, 192, 168, 10, 10);
210             err2 = netconn_connect(conn_client, &ipremote, 5000);
211             if(err2 == ERR_OK){
212               conn_wifi=conn_client;
213               xTaskCreate( tcpclient_wifi, "tcp_client_WiFi",
configMINIMAL_STACK_SIZE * 5, NULL, 1, NULL );
214             }
215         }
216 }
217
218 void setup() {
219
220     bool ret;
221
222     Serial.begin(115200);
223
```

```
224     Serial.println();
225     Serial.println();
226     Serial.print("Connecting to ");
227     Serial.println(ssid);
228
229     WiFi.begin(ssid, passphrase);
230
231     while (WiFi.status() != WL_CONNECTED) {
232         delay(500);
233         Serial.print(".");
234     }
235
236     Serial.println("");
237     Serial.println("WiFi connected");
238     Serial.println("IP address: ");
239     Serial.println(WiFi.localIP());
240
241     tcpip_adapter_init();
242     tcpip_adapter_dhcpc_stop(TCPIP_ADAPTER_IF_ETH); // Don't run a DHCP
client
243     tcpip_adapter_ip_info_t ipInfo;
244     ip4addr_aton(IP_DEFAULT_ADDRESS_ETH, &ipInfo.ip);
245     ip4addr_aton(IP_DEFAULT_GATEWAY_ETH, &ipInfo.gw);
246     ip4addr_aton(IP_DEFAULT_NETMASK_ETH, &ipInfo.netmask);
247     ESP_ERROR_CHECK(tcpip_adapter_set_ip_info(TCPIP_ADAPTER_IF_ETH,
&ipInfo));
248
249     //ESP_ERROR_CHECK(esp_event_loop_init(NULL, NULL));
250
251     eth_config_t phyConfig = DEFAULT_ETHERNET_PHY_CONFIG;
252     phyConfig.phy_addr = PHY0;
253     phyConfig.gpio_config = eth_gpio_config_rmii;
254     phyConfig.tcpip_input = tcpip_adapter_eth_input;
255     ESP_ERROR_CHECK(esp_eth_init(&phyConfig));
256     ESP_ERROR_CHECK(esp_eth_enable());
257
258     ESP_ERROR_CHECK(tcpip_adapter_get_ip_info(TCPIP_ADAPTER_IF_ETH,
&ipInfo));
259     printf("main: Network started on "IPSTR"\n", IP2STR(&ipInfo.ip));
260
261     wifi_connection();
262
263     tcpecho_init();
264
265     pinMode(pushButton, INPUT);
266 }
```

```
267 int len_sensor, k;
268 float voltage;
269 char data_sensor[50];
270 
271 void loop(){
272 
273     if (WiFi.status() != WL_CONNECTED){
274       Serial.println("WiFi disconnected");
275       WiFi.begin(ssid, passphrase);
276 
277       while (WiFi.status() != WL_CONNECTED) {
278           delay(500);
279          Serial.print(".");
280       }
281       Serial.println("");
282       Serial.println("WiFi connected");
283       Serial.println("IP address: ");
284       Serial.println(WiFi.localIP());
285     }
286 }
```